5-2017

Water Entry Impact Dynamics of Diving Birds

Saberul Islam Sharker
Utah State University

WATER ENTRY IMPACT DYNAMICS OF DIVING BIRDS

by

Saberul Islam Sharker

A thesis submitted in partial fulfillment
of the requirements for the degree

of

MASTER OF SCIENCE

in

Mechanical Engineering

Approved:

Tadd T. Truscott, Ph.D. Major Professor	Robert E. Spall, Ph.D. Committee Member
Ryan Berke, Ph.D. Committee Member	Mark R. McLellan, Ph.D. Vice President for Research and Dean of the School of Graduate Studies

UTAH STATE UNIVERSITY
Logan, Utah

2017

ABSTRACT

Water Entry Impact Dynamics of Diving Birds

by

Saberul Islam Sharker, Master of Science

Utah State University, 2017

Major Professor: Tadd T. Truscott, Ph.D.
Department: Mechanical and Aerospace Engineering

Some seabirds (such as Northern Gannets and Brown Boobies) can dive from heights as high as 30 m reaching speeds of up to 24 m/s as they impact the water surface. It is perceived that physical geometry, particularly of the beak, allows them to endure relatively high impact forces that could otherwise kill non-diving birds. Acceleration data from simplified models of diving birds agree with simulated data for one species (Northern Gannet), however, no reliable experimental data with real bird geometries exist for comparison purposes. This study utilizes eleven 3D printed diving birds (five plunge-diving, five surface-diving and one dipper) with embedded accelerometers to measure water-entry impact accelerations for impact velocities ranging between 4.4 - 23.2 m/s. Impact forces for all bird types are found to be comparable under similar impact conditions and well within the safe zone characterized by neck strength as found in recent studies. However, the time each bird requires to reach maximum impact acceleration and its effect represented here by the derivative of acceleration (i.e., jerk), is different based on its beak and head shape. We show

that surface diving birds cannot dive at high speeds as the non-dimensional jerk experienced exceeds a safe limit estimated from human impact analysis, whereas those by plunge divers do not.

(56 pages)

PUBLIC ABSTRACT

Water Entry Impact Dynamics of Diving Birds

Saberul Islam Sharker

Plunge diving and surface diving are two main techniques used by seabirds for foraging purposes. While some plunge divers can dive into the water at very high speeds (24 m/s), surface divers do not. This study analyzes the free-surface impact of 3D printed bird head models with embedded accelerometers to determine why surface divers cannot dive safely at high speeds. The problem is investigated in the context of impact jerk where surface divers, unlike plunge divers, are found to experience non-dimensional jerk (J^*) values exceeding a safe limit. This approach portrays itself as an unconventional yet effective method for differentiating between seabird species and can also be employed for estimating maximum safe impact speeds in other organisms.

ACKNOWLEDGMENTS

I would like to express my gratitude to those who have stood beside me, encouraged me and lent their assistance. First, I would like to sincerely thank my supervisor, Dr. Tadd Truscott, for his valuable guidance, suggestions and constant supervision throughout the completion of the project. Without his continuous help, it would have been impossible for me to do all these work. I thank him very much for all his precious time given to me. I would also like to acknowledge the constructive criticisms of my colleagues at the Splash Lab and all the help they provided throughout the experiments.

I also wish to express my appreciation to the Delaware Museum of Natural History and Jean Woods (Curator of Birds) for access to their ornithological collection; Danielle Adams, William Gough, and Kelsey Tennett for assistance with 3D scanning; Troy Ovard for providing access to the Upper Stillwater Dam; Terry Zollinger for helping at the machine shop; and Dr. Frank Fish from the West Chester University for bringing the problem to our attention and providing us the bird scans.

Finally, I want to say that I am indebted to my family and friends for their love, support and encouragement throughout my education and always being there for me.

Saberul Islam Sharker

CONTENTS

LIST OF TABLES

LIST OF FIGURES

CHAPTER 1

INTRODUCTION

As an object enters into a body of fluid, it experiences an impact force which depends primarily on the impact velocity, shape and the density of the material among other factors. The impact force measurements can be important for a number of applications, including water slamming of boats and certain military applications which require transition from air to water. Another interesting example in nature is the impact dynamics of seabirds. Many previous studies have investigated the water impact of canonical shapes, but very few authors have focused on seabirds. This thesis presents findings from the analysis of the water impact of seabirds at high speeds.

1.1 Background

1.1.1 Canonical Shapes

The water impact of canonical shapes such as spheres and cones can be divided into a number of distinct phases [1, 2]: 1. shock-wave phase (Fig. 1.1 frame 1), 2. flow-forming phase, 3. open-cavity phase (frame 2), 4. closed-cavity phase (frame 5), 5. collapsing cavity phase (pinch-off, frame 11), and 6. fully-wetted phase (not shown). Studies of the impact of a solid on a liquid surface have been mainly of two kinds, those which are concerned with the force of impact (phase 1), and those which are concerned with the formation of the cavity and splash (phases 2-6). One of the earliest theoretical calculations of the impact force of a sphere has been made by Schiffman and Spencer [3] which was later verified experimentally by Moghisi and Squire [4]. According to the Schiffman-Spencer theory, as a sphere falls vertically

into a pool of liquid, the stage of impact under consideration is before separation has commenced and when the depth of the sphere under water is less than half its radius. For low viscosity liquids, the impact force is proportional to the impact velocity squared, and directly proportional to the impact velocity in the case of high viscosity liquids. The impact force rises rapidly to a maximum when the depth of penetration is between a tenth and a fifth of the radius of sphere. The force declines more gradually towards a value of between 0.25 and 0.3 when the cavity is fully formed, as found by May and Woodhull [5]. Truscott, Epps and Techet [6] observed a decrease in the acceleration of an impacting sphere immediately prior to pinch-off. This force arises as the impacting body experiences a net upward force upon impact due to the effects of momentum transfer to the liquid, surface tension, viscous drag and pressure forces [7]. Experimental studies of projectiles [3, 4, 8, 9] show that the forces of blunt body water entry can be maximum anywhere between phases 1 and 5. Thus, the forces of the initial stages of impact must be measured in order to make estimates of the dynamic strength for a given structure [10].

Fig. 1.1: The water entry of a steel sphere [6] showing the different phases from impact to pinch-off.

Experiments performed with different projectile shapes [9] show that nose shape of the projectile has a major effect on the impact force during water entry. They used three different nose shapes: flat, cone and ogive. The impact forces measured

for a flat nose projectile at vertical entry were significantly higher than those of other two due to the blunt flat geometry. This force was reduced appreciably (almost by half) when the projectile impacted water at an angle of 5 degrees. The ogive nose shape experienced slightly higher impact force than the cone shape projectiles but still nearly half as much when compared to the flat nose. When the cone and ogive projectiles were released with an impact angle of 5 degrees, they had almost the same amount of impact force as vertical entry. At impact, there is an increase in axial acceleration, but there is no significant change in the radial acceleration, showing that most of the impact acceleration occurs in the axial direction. Tveitnes et al [11] performed similar experiments but with wedge-shaped sections of different deadrise angles. They found that, for the same deadrise angle, increasing the impact velocity increases the maximum force while increasing the deadrise angle with a constant impact velocity, decreases the force.

1.1.2 Diving Birds

Seabirds have adapted well to survive in the marine environment. These birds feed mostly on fish, catching their prey mainly in two different ways: surface diving and plunge diving. Birds like the Common Loon and the Double-crested Cormorant rest on the surface of the water and then dive when they target their prey, hence called surface divers. On the other hand, specialized plunge divers such as the Northern Gannet and the Brown Booby can dive from heights as high as 30 m reaching speeds of 24 m/s as they impact the water [12] while folding their wings to minimize the impact force and conserve momentum [13,14]. Some birds, like the Herring Gull, feed by dipping [15] and get their food any way they can, mainly by scavenging or picking fish from the surface. Herring Gulls are also occasionally seen to make shallow plunge dives [16, 17] but are not classified as plunging specialists. Plunge diving birds are

able to dive 1.2 to 12.6 m in depth and a further 22 m by active flapping [14, 18–20]. Although plunge diving is a highly successful technique for catching food, it does not always end with a hearty meal. Diving at these high speeds can sometimes be fatal as the birds can collide with one another [21].

The negative accelerations associated with impact reported in limited studies on plunge diving birds appear contradictory. Numerical simulations performed by Wang *et al.* [22] found very large deceleration values at impact (23 times gravitational acceleration, g, for an impact velocity of 24 m/s) resulting in considerable water entry forces on the gannet body. On the other hand, experiments by Ropert-Coudert *et al.* [12] found zero to very small decelerations during the impact stage of water entry. They attached data loggers to the back of the neck and tail of Norther Gannets but the sampling frequency (32 Hz) may have been too low to detect the short duration impact event. Thus, higher sampling frequency experiments are required to accurately record the impact dynamics.

The neck is potentially the most vulnerable part of the bird especially when diving. Recent studies [23] have revealed Brown Boobies and Northern Gannets may be well within the safe limits of neck failure. Chang *et al.* attached an elastic beam to a cone representing the bird neck and skull. The bending forces on the elastic beam were measured as the cone-beam system was dropped into water with impact velocities ranging from 0.5 to 2.5 m/s. An unstable and a stable region were identified and theoretical analogs from the empirical data indicated that these birds dive well within their safe neck bending limits.

1.2 Objective

This study focuses on the initial phases of impact for eleven birds (5 plunge divers, 5 surface divers and 1 dipper). These 3D printed bird heads are used to analyze the

water-entry dynamics with embedded accelerometers to measure impact accelerations. Studying the free-surface impact forces in relation to the birds physical features gives insight into understanding the properties that explain why plunge diving birds dive underwater at high speeds but surface diving birds do not, although both types of birds have similar feeding niches.

CHAPTER 2

EXPERIMENTAL METHODS

The impact dynamics of five plunge diving, five surface diving birds and one dipper were experimentally investigated during water entry at different impact velocities ranging between $4.4 - 23.2$ m/s. 3D scanned models of real birds were used in the experiment with embedded accelerometers of a high sampling frequency of 1000 Hz. Due to the large heights required for drops, most of the experiment was done outdoors with limited capabilities of equipment that can be used.

2.1 Birds

Specimens of five plunge diving, five surface diving birds and one dipper (Table 2.1) were obtained from the Delaware Museum of Natural History. Heads of the birds were 3D scanned with the GoMeasure 3D HDI Advance R1 scanning system (Amherst, VA). The scans reflected an accurate model of live bird heads as the specimens included both the beak and the skull. The posterior parts of the scans were modified (using MeshLab and SolidWorks software) to incorporate an internal accelerometer near the neck region (Figure 2.1c) and the corresponding drawings were made to resemble the contour of real birds as closely as possible. The birds were then 3D printed and treated with acetone to smooth out imperfections from 3D printing. The properties of the 3D printed bird models are presented in Table 2.2. Since the printed bird heads had a heavier rear end which made them prone to rotate during free-fall, a long shaft with fletching (i.e., arrow) was attached to their backside for stabilizing purposes as shown in Figure 2.1e.

Table 2.1: List of birds used and their physical properties. Data has been collected from Alderfer [24] and Perrins [25].

Name of Bird	Mass [kg]	Length [cm]	Dive height [m]
Plunge Diving Birds			
Belted Kingfisher (*Megaceryle alcyon*)	0.14 to 0.17	28 to 35	10 to 12
Brown Booby (*Sula leucogaster*)	1.00 to 1.80	64 to 85	15 to 20
Common Tern (*Sterna hirundo*)	0.10 to 0.20	31 to 38	1 to 6
Northern Gannet (*Morus bassanus*)	2.20 to 3.60	81 to 110	10 to 30
Red-footed Booby (*Sula sula*)	0.85 to 1.10	69 to 79	10 to 30
Dipper			
Herring Gull (*Larus argentatus*)	0.80 to 1.25	56 to 66	1 to 12
Surface Diving Birds			
Atlantic Puffin (*Fratercula arctica*)	0.40 to 0.65	28 to 30	0
Common Eider (*Somateria mollissima*)	1.92 to 2.21	50 to 71	0
Double-crested Cormorant (*Phalacrocorax auritus*)	1.20 to 2.50	70 to 90	0
Common Loon (*Gavia immer*)	2.50 to 6.0	66 to 91	0
Red-breasted Merganser (*Mergus serrator*)	0.80 to 1.35	51 to 64	0

Table 2.2: Physical properties of the 3D printed bird heads. The mass is the combined mass of the printed bird and the IMU.

Name of Bird	Mass [kg]	Beak Length [mm]	Neck Diameter [mm]
Plunge Diving Birds			
Belted Kingfisher	0.375	68.8	41.1
Brown Booby	0.292	95.1	48.2
Common Tern	0.377	76.0	29.2
Northern Gannet	0.452	102.4	68.0
Red-footed Booby	0.251	69.7	48.9
Dipper			
Herring Gull	0.452	54.8	68.1
Surface Diving Birds			
Atlantic Puffin	0.349	44.4	41.7
Common Eider	0.292	59.0	52.3
Double-crested Cormorant	0.248	62.8	40.5
Common Loon	0.349	74.5	58.2
Red-breasted Merganser	0.263	63.0	49.8

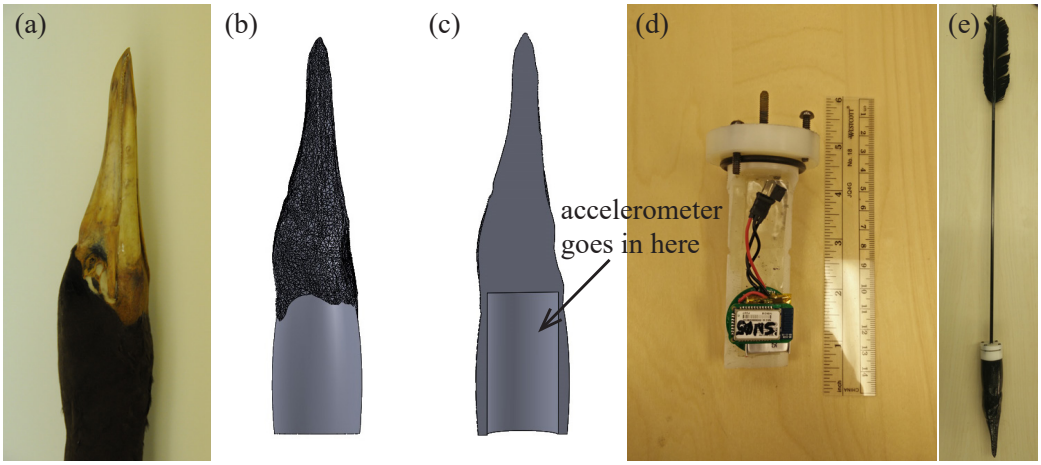

Fig. 2.1: (a) Actual picture of a Brown Booby for comparison of beak and neck profiles with modified drawings. (b) Side view of the modified Brown Booby drawing that was 3D printed, (c) Sectional view, showing space for the internal accelerometer container, (d) The Inertial Measurement Unit (IMU) in its waterproof container, (e) 3D printed bird with a long shaft and fletching for stabilization.

2.1.1 Measurement of Beak angle

The beak angle of a bird can be different depending on which direction it is looked upon. They usually have two distinct beak angles: one from the top view and the other from the side view. These angles are measured on the printed bird heads using ImageJ software, as shown in Figure 2.2 for one specimen, Belted Kingfisher.

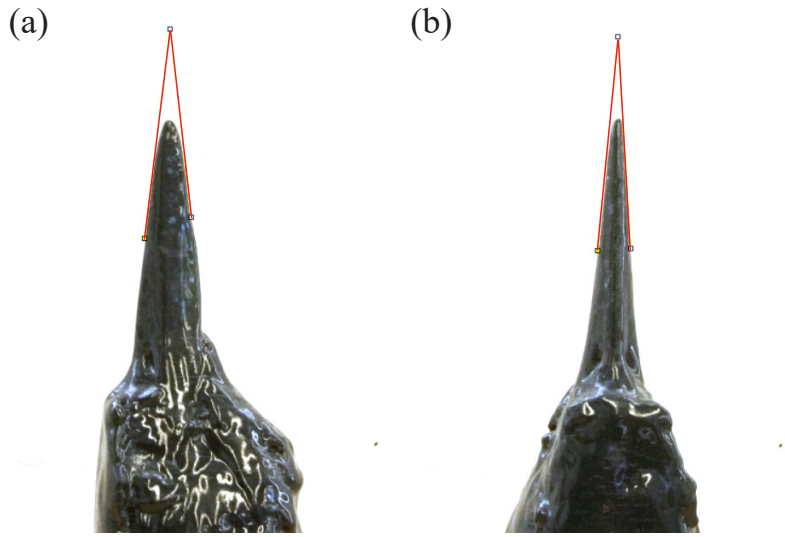

Fig. 2.2: (a) Side angle and (b) top angle of a Belted Kingfisher, outlined by red lines. Angles are measured using ImageJ software.

2.2 Setup

The printed birds were dropped from heights as high as 30 m reaching speeds of up to 23.2 m/s. Maximum drop heights of only 1 m were permissible in the laboratory where the 3D printed bird models and embedded accelerometers were dropped vertically from an electromagnet into a glass tank containing water and the events were recorded using high-speed cameras (Photron SA3, 1000 fps) both below and above the water surface. Higher impact velocities were achieved in a 4.7 m deep swimming pool at USU while the highest drop heights were conducted at

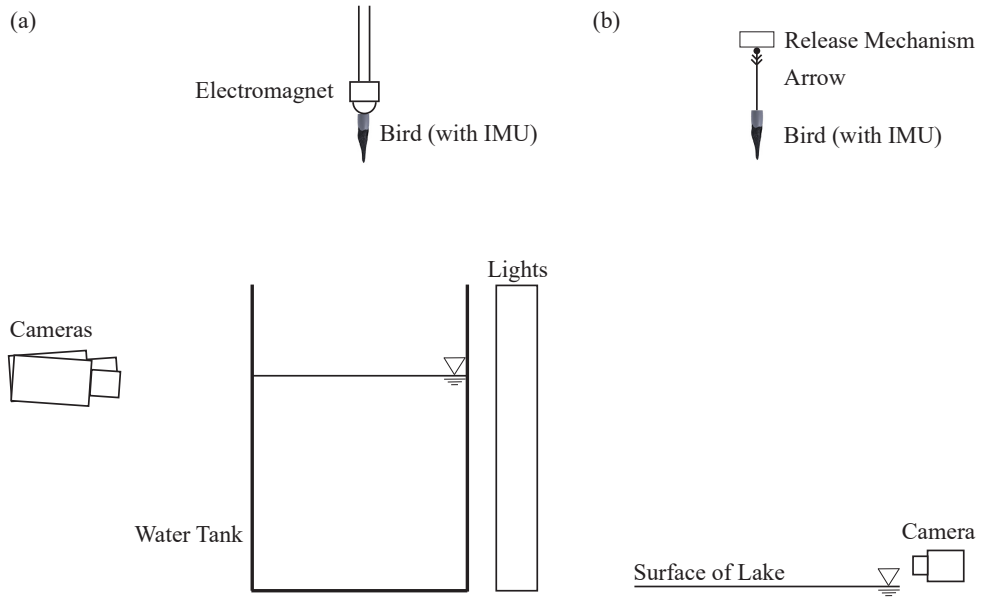

Fig. 2.3: Schematic of the experimental setup. (a) The bird head model containing the IMU was released vertically from an electromagnet while two high-speed cameras captured the water entry event from above and below the free surface. (b) High impact velocity experiments were performed in a pool or a lake with a camera viewing from above the free surface to capture the bird's fall.

the Upper Stillwater Dam in Duchesne County, Utah. The 3D printed models and accelerometers in these cases were lifted to the desired height and released using a remote release mechanism (Figure 2.3b). At the pool, a high speed camera (Photron SA3, 500 fps) was used for viewing from below the surface, while a 120 fps camera (Sony Alpha 7r) was used above the surface (1 m) at both the pool and the lake for impact speed calculations.

2.3 Inertial Measurement Unit (IMU)

An Inertial Measurement Unit (InvenSense MPU-9250) consisting of a 3-axis accelerometer, a 3-axis gyroscope and a 3-axis magnetometer was embedded in the bird heads. MPU-9250 is a multi-chip module (MCM) consisting of a gyroscope, an accelerometer and an electronic compass (Asahi Kasei Microdevices AK8963).

The MPU-9250 accelerometer has a maximum range (16g) lower than our expected maximum, hence an additional accelerometer (ST H3LIS331DL) with a maximum range of 400g was added to the unit. Both accelerometers had sampling frequencies of 1000 Hz to measure the impact accelerations of the bird heads. The wireless IMU (Figure 2.1d) was connected to a computer via Bluetooth and triggered manually or by detecting freefall to start data recording. The unit was placed securely in a waterproof container within the printed birds as shown in Figure 2.1c.

2.3.1 Zero-offset Bias Removal from Accelerometer Data

The measured data from the accelerometer should nominally read $0g$ on all axes during free-fall. The raw data from the accelerometer showed an offset from the zero value during free-fall. It was necessary to remove the zero-offset bias from the acceleration data before performing calculations. The zero-offset bias was determined by calculating the mean of the free-fall portion of the data and subtracting the result

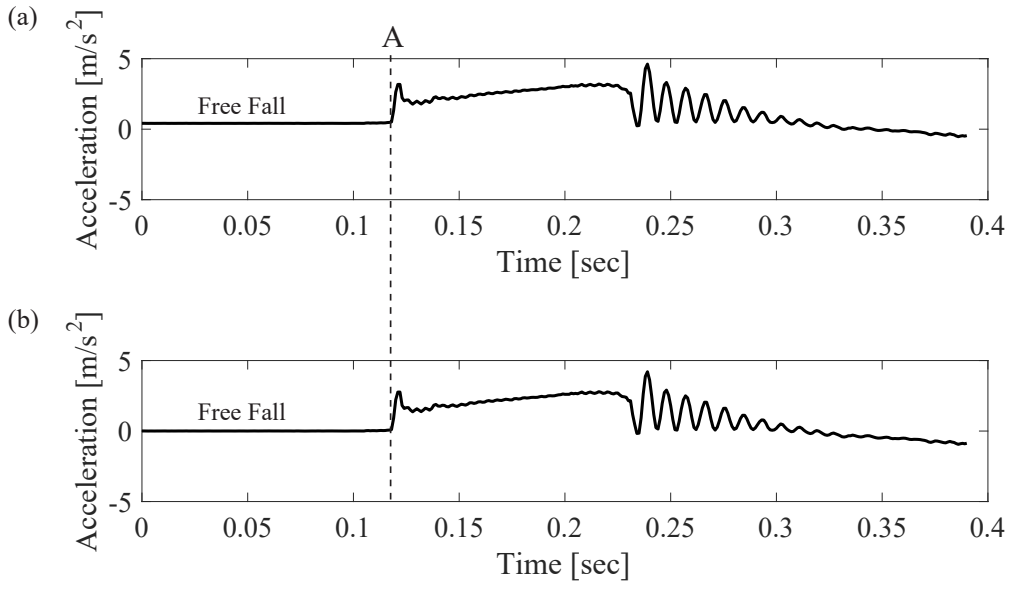

Fig. 2.4: Acceleration data showing the free-fall region and impact (A). (a) shows the plot before zero-offset bias removal, and (b) shows the corrected plot after removal.

from the rest of the water entry event. Figure 2.4 shows the axial acceleration data before and after correcting the zero-offset error.

2.3.2 Velocity from Accelerometer Data

The acceleration data were integrated numerically using the trapezoidal method in MATLAB to compute velocity and then integrated again to compute position, if needed, following the equation:

$$\int_a^b f(x)\,dx \approx \frac{f(a)+f(b)}{2}(b-a) \tag{2.1}$$

where $f(a)$ is the acceleration (or velocity) value at the first instant in time and $f(b)$ is the acceleration (or velocity) value at the final instant in time.

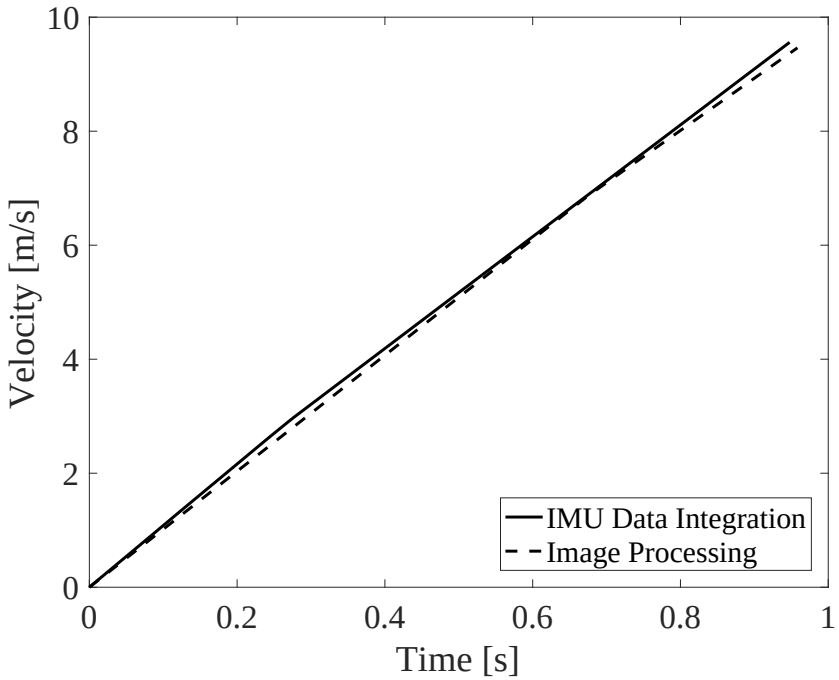

Fig. 2.5: Validation of the IMU with velocities obtained from image processing and from IMU data integration. The maximum value of velocity presented here is the impact velocity.

2.3.3 IMU Validation

Data from the IMU was validated against measurements obtained by image processing. As the bird heads were dropped into a body a water, the fall was captured using a camera with a frame rate of 120 fps. The impact velocity was measured from the images using image processing techniques in MATLAB. The free-fall region in the data from the IMU was integrated, as explained above, to obtain the velocity. A comparison of the velocities obtained from IMU and from image processing for a drop from 5 meters is presented in Figure 2.5. The maximum value of velocity obtained is the impact velocity. It is seen that the velocities calculated in such ways are very close to each other.

2.4 Release Mechanism

A remote controlled servo controls a lever which, in its outward position, holds the bird vertically. As the trigger is pulled, the servo makes the lever move inwards which releases the bird into the body of water (Figure 2.6). Data from the accelerometer can be extracted once the bird is retrieved from the water.

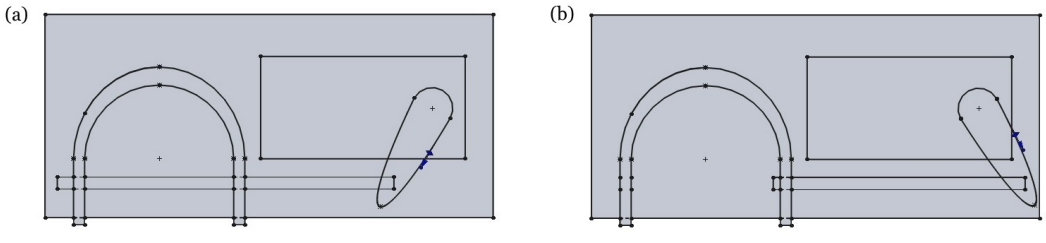

Fig. 2.6: Positions of the release mechanism. (a) shows the device in its closed position that will hold the bird so that it can be carried to the desired height, (b) shows the device when it is opened, so that the bird drops when triggered remotely.

CHAPTER 3

RESULTS AND DISCUSSION

Five plunge diving, one dipper, and five surface diving bird models were released into water with impact velocities ranging between $4.4 - 23.2\ m/s$ (properties listed in Table 2.2). Image sequences in Figure 3.1, Figure 3.2 and Figure 3.3 demonstrate the water entry events of three plunge diving birds (Common Tern, Brown Booby and Red-footed Booby), three surface diving birds (Atlantic Puffin, Common Loon and Double-crested Cormorant) and the dipper (Herring Gull) respectively. Air entrainment and cavity formation occurs as the bird heads impact the water surface and travel through the fluid.

3.1 Bird Heads vs Cones

Previous literature used cones as an approximation to bird heads [23]. Trends in impact acceleration noted by Bodily *et al.* [9] for projectiles with conical and ogive noses resemble accelerometer results obtained for seabird models in this study. However, comparing maximum drag coefficients obtained here to those of cones from experiments by Baldwin [26] reveals different results as shown in Figure 3.4. The maximum drag coefficient for the birds is calculated as:

$$C_d = \frac{F}{\frac{1}{2}\rho v^2 A_b} \tag{3.1}$$

where C_d is the maximum drag coefficient, F is the maximum force experienced by the bird head model, ρ is the density of water, v is the impact velocity and A_b is the projected frontal area of the bird beak. A noticeable difference in C_d for birds

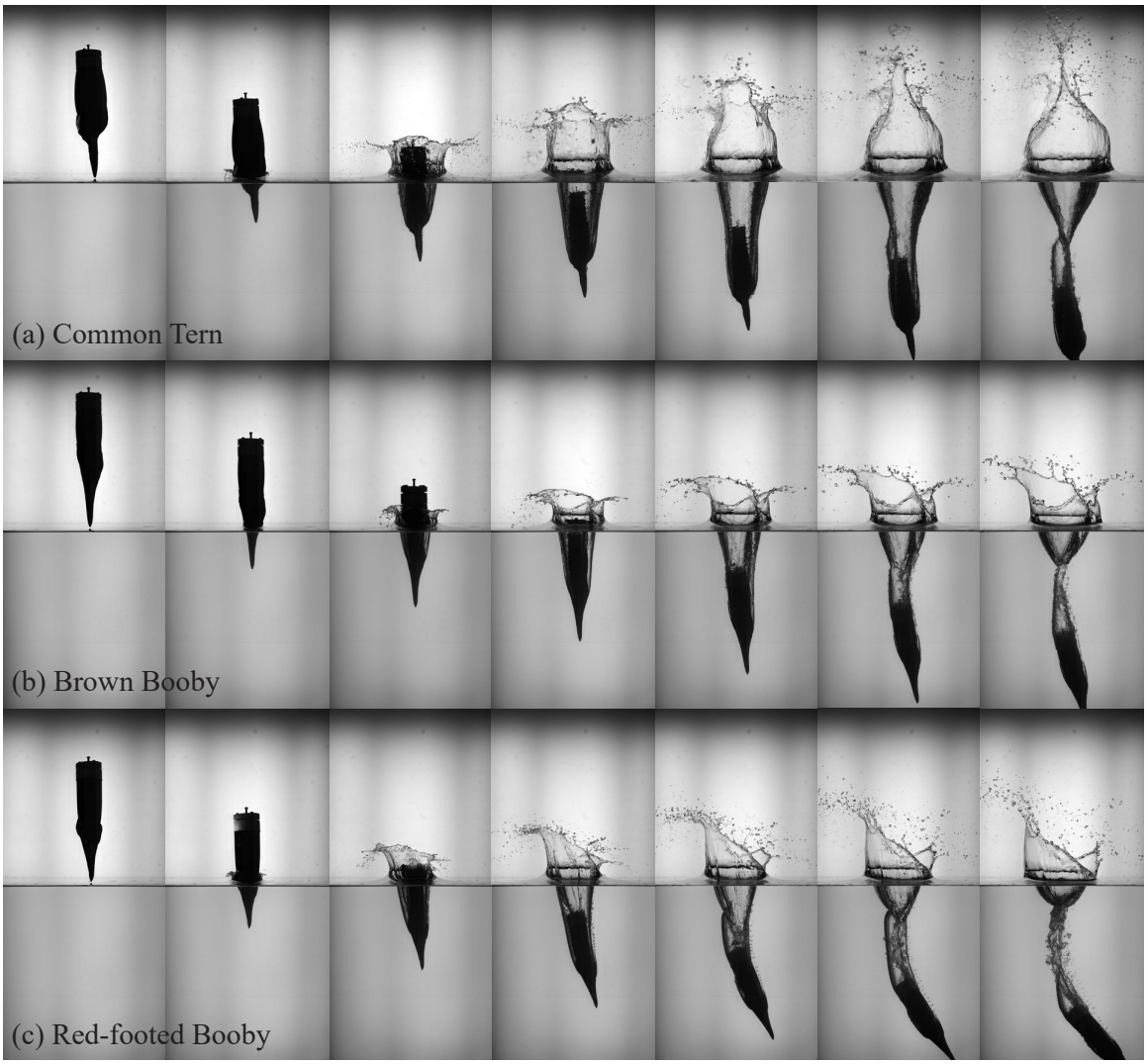

Fig. 3.1: Image sequences showing the water entry of three plunge diving birds as marked for an impact velocity of $v = 4.4$ m/s. The time interval between each image is 22 ms. Birds are imaged from the side profile with eyes on the right. All birds pitch upward after impact.

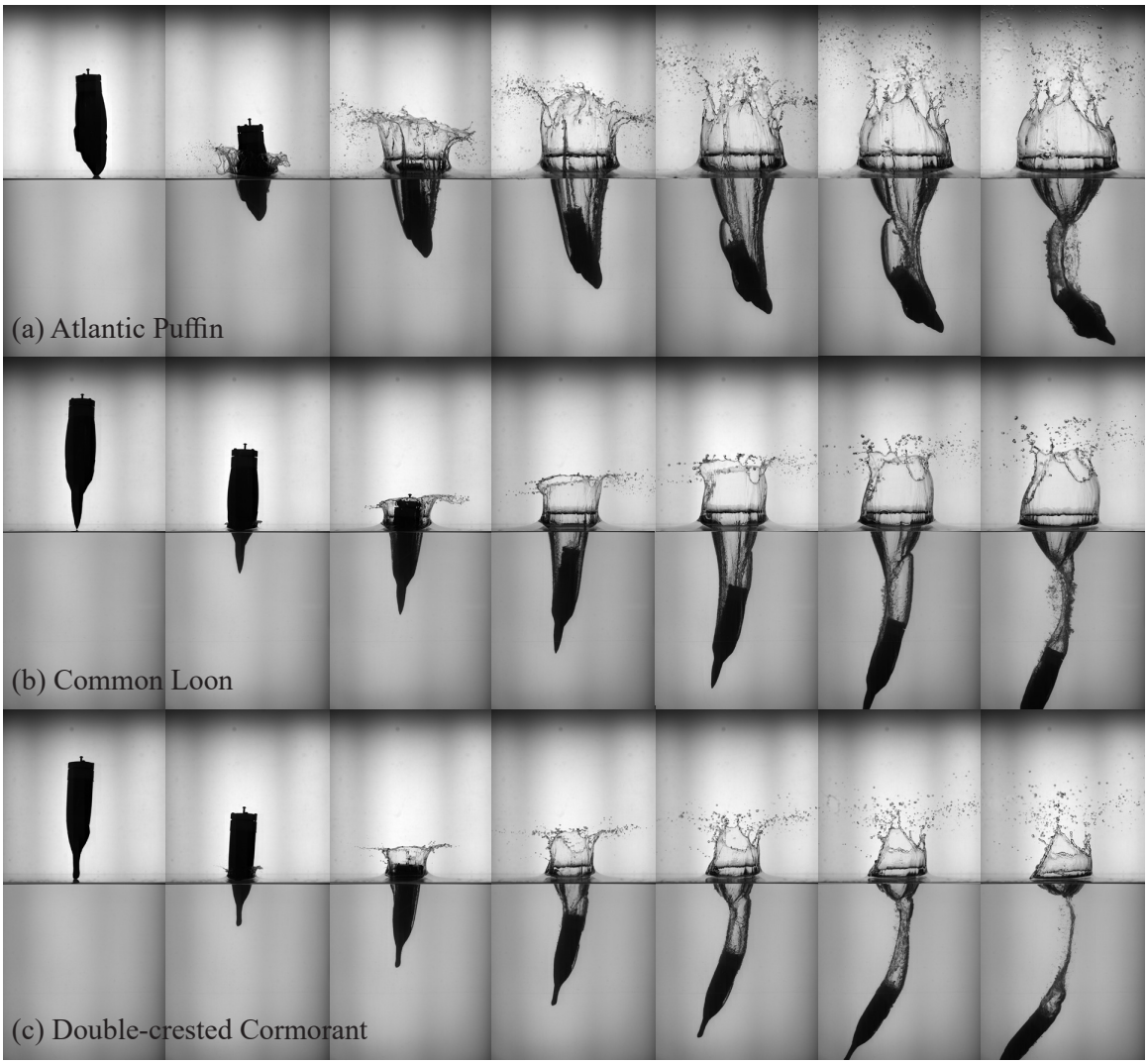

Fig. 3.2: Image sequences showing the water entry of three surface diving birds as marked for an impact velocity of $v = 4.4$ m/s. The time interval between each image is 22 ms. Birds are imaged from the side profile with eyes on the right. The Atlantic Puffin pitches upward, whereas the Common Loon and the Double-crested Cormorant pitch downward, after impact.

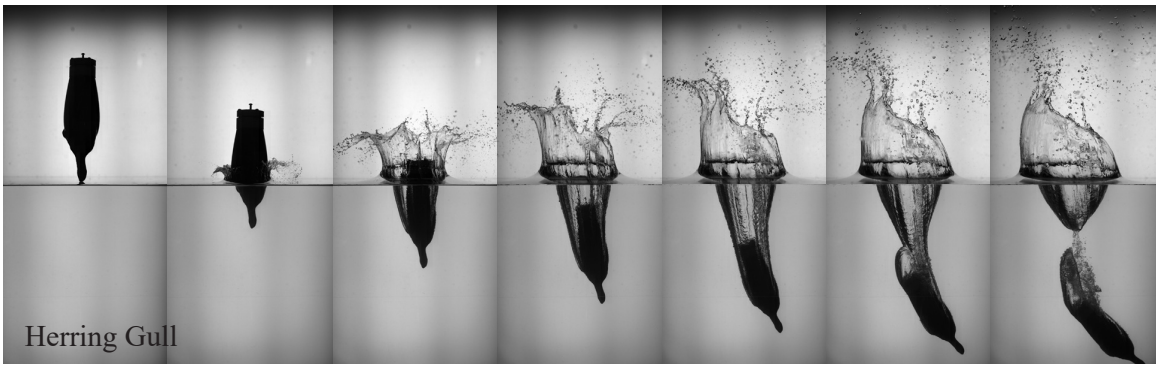

Fig. 3.3: Image sequences showing the water entry of the dipper (Herring Gull) for an impact velocity of $v = 4.4$ m/s. The time interval between each image is 22 ms. The bird is imaged from the side profile with eyes on the right. The Herring Gull pitches upward after impact.

with similar beak angles is evident. The largest beak angle for each bird in this regard is used for comparison purposes. The difference arises from bird heads having varying beak angle values in the azimuthal plane, unlike cones which are uniformly shaped objects. Hence, instead of approximating bird heads as cones, exact 3D printed replicas are used in the current experiment for more accurate results.

3.2 Beak Angle Ratio

Most bird beaks have two distinct angles, one of which can be measured from the side view, and the other from the top view. In this study, we use a ratio of the smaller-to-larger beak angles, called the beak angle ratio as presented in Figure 3.5. High beak angle ratios (e.g., Red-footed Booby) result from top and side angles being in close proximity while low beak angle ratios (e.g., Atlantic Puffin) occur when the difference is greater. The dotted line separates birds based on their beak angle ratios: plunge diving birds fall above the line, while the dipper and the surface diving birds lie below the line with one exception, the Merganser. It is a surface diver with a beak characterized by a round tip and thus a high beak angle ratio of 1 (see Appendix A Figure A.2).

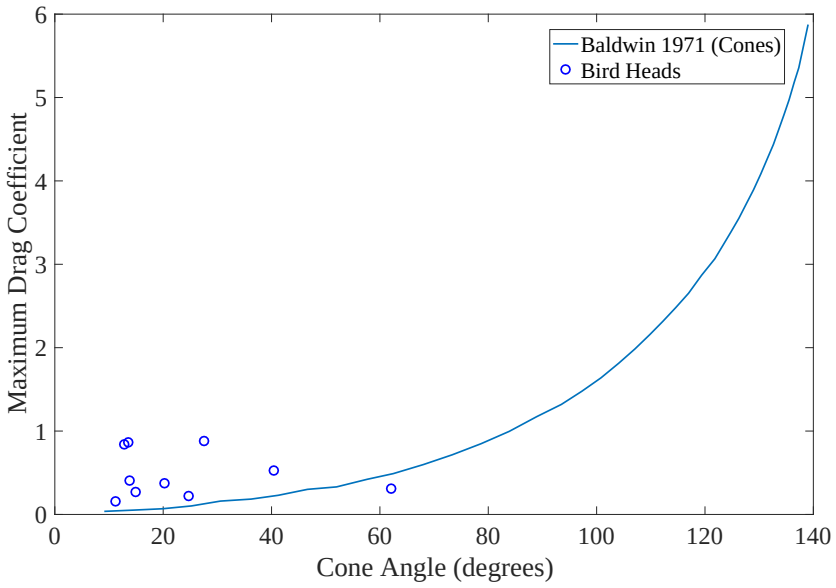

Fig. 3.4: Maximum drag coefficient C_d of cones versus cone angles as obtained by Baldwin [26] in comparison with those obtained for bird heads in this study.

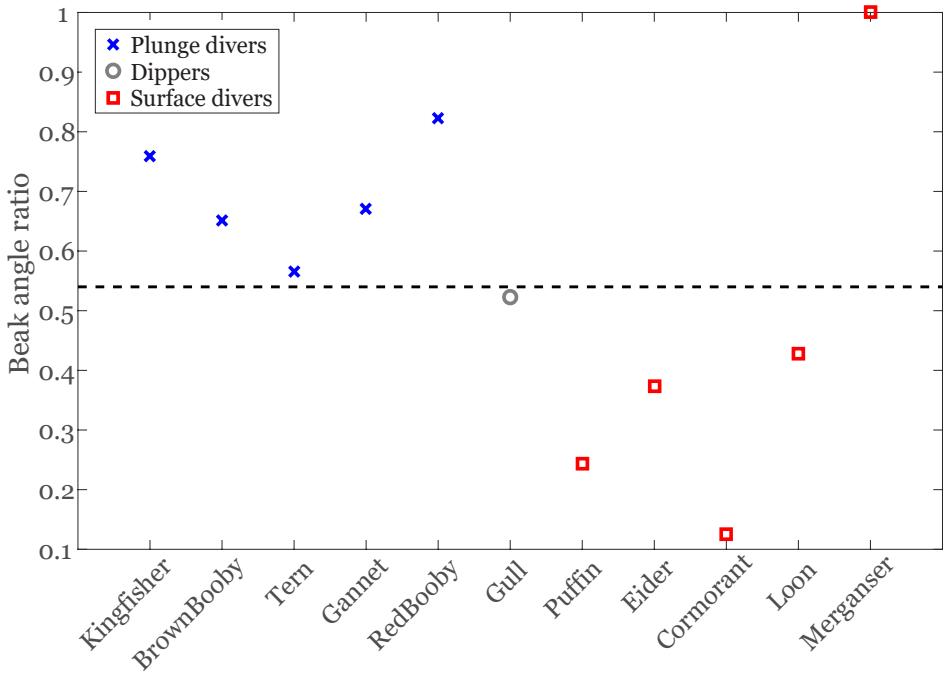

Fig. 3.5: Beak angle ratios of dipper, surface and plunge diving birds. The dotted line separates plunge divers from the dipper and surface divers.

3.3 Impact Acceleration

Bird head water entry image sequences were synchronized with accelerometers for all but the highest impact speeds where only accelerometers were used. Figure 3.6a shows an image-sequence for a plunge diving bird, the Northern Gannet, as it enters water (A) at an impact velocity of 4.4 m/s until the cavity pinches-off (C). Impact acceleration recorded by the accelerometer in Figure 3.6b-d (a_x, a_y, a_z, respectively) is experienced more prominently in the axial direction as indicated by the sudden increase in acceleration after the free-fall region (A) in Figure 3.6b, and the lack of any significant acceleration in radial directions in Figure 3.6c & d. The second peak appears after the cavity pinches-off (C), causing pressure reverberations typical of cavity collapse as shown by Grumstrup *et al.* [27]. The reverberations decay through the remainder of the descent of the projectile. Continued oscillations are seen from the accelerometer data and the frequencies of these oscillations can vary for the bird heads at different impact velocities as observed for different projectile shapes by other authors. In general, the frequencies of the oscillations are similar for all bird heads at the same impact speed, but as the speed increases, the frequency decreases (see Appendix B Table B.1). Grumstrup *et al.* [27] showed oscillation frequencies of 190 Hz for a sphere of diameter = 0.01905 meter impacting at 4 m/s, whereas Bodily *et al.* [9] found frequencies of 208.5 Hz, 210.9 Hz, and 212.7 Hz for cone, ogive, and flat nose projectiles, respectively, at impacting at 2.7 m/s. The collapse of the cavity affects the projectile acceleration in all directions with the largest change occurring in the axial direction. The images also show a pitch down trajectory as the bird travels downward through the water column. This causes the rear end of the bird model to touch the cavity walls (B), disrupting the cavity shape.

A measure of the impact force experienced by the 3D printed bird heads can be obtained by comparing impact accelerations, a, during water-entry. The impact

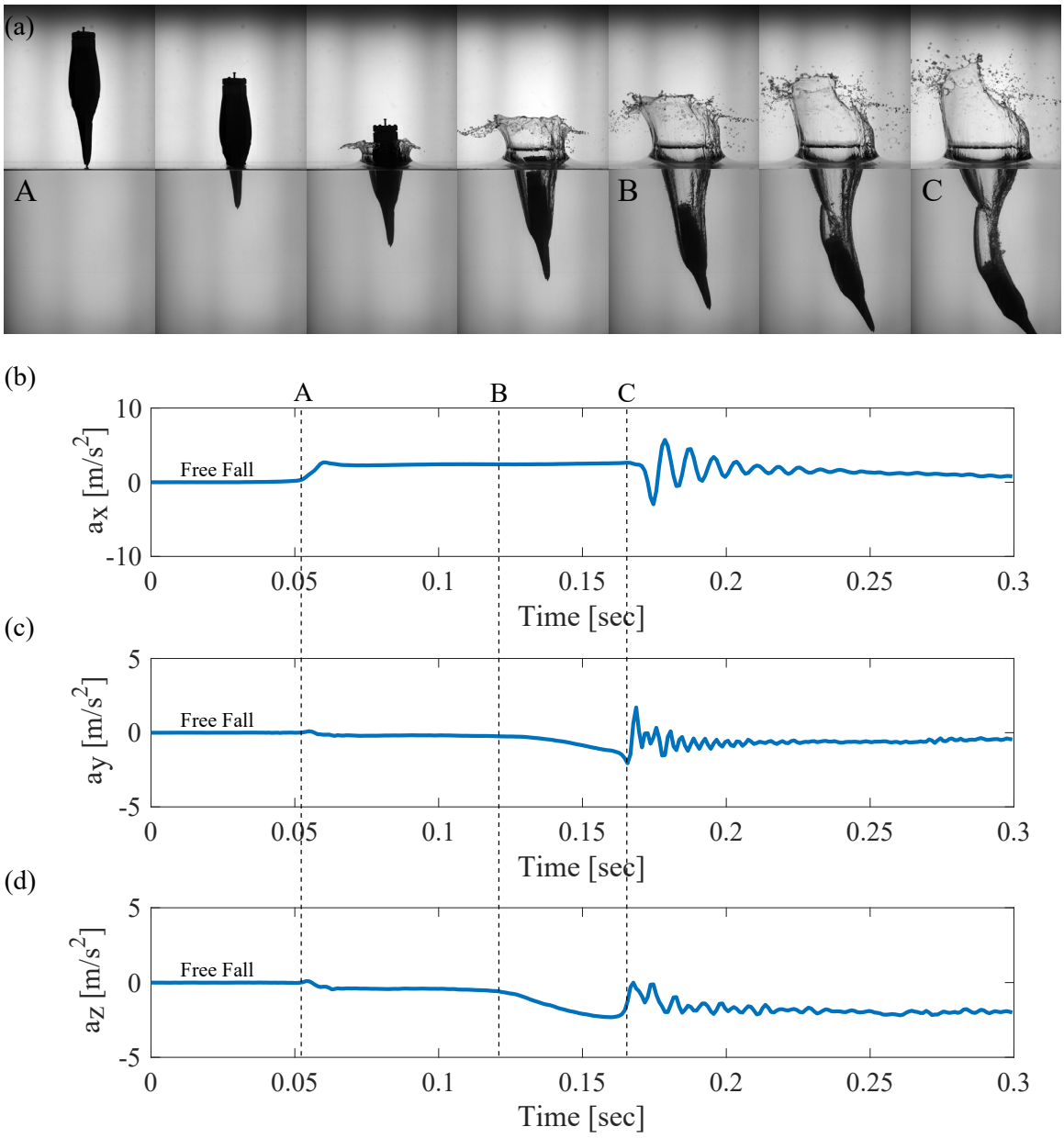

Fig. 3.6: (a) Water-entry event of the Northern Gannet for an impact velocity of $v = 4.4$ m/s. The time interval between each image is 22 ms. Axial acceleration data (b) is synchronized with the two radial acceleration data (c & d). Capital letters represent stages of the impact: (A) impact with water, (B) change in radial acceleration from the bird model rear end touching the cavity walls, and (C) cavity pinch-off.

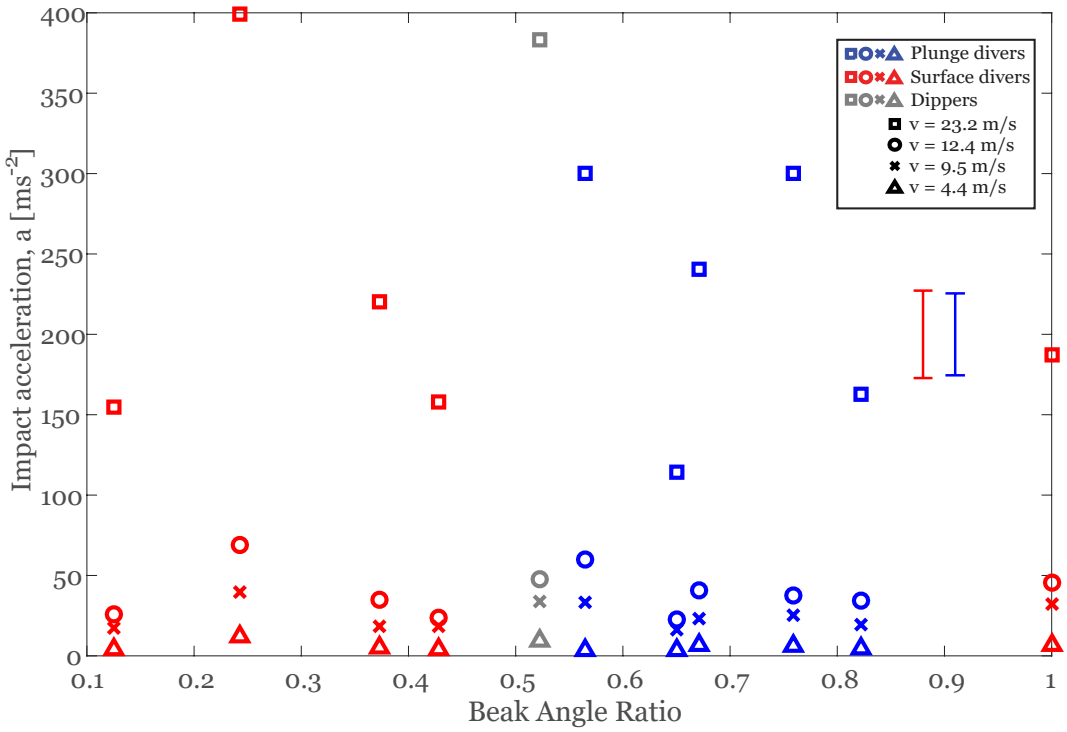

Fig. 3.7: Impact accelerations recorded by the Inertial measurement unit (IMU) vs beak angle ratios of the bird head models used for four different impact velocities. The error bars represent the largest measurement errors.

accelerations of all bird heads with impact velocities ranging between $4.4 - 23.2\ m/s$ are shown in Figure 3.7 where the first peak in acceleration directly after impacting the water surface (e.g., at A in Figure 3.6b) represents the impact acceleration. Although accelerations in the radial direction are much lower than those in the axial direction, the overall impact acceleration considered is a measure of accelerations in all three directions of the accelerometer axes.

$$a = \sqrt{a_x^2 + a_y^2 + a_z^2} \tag{3.2}$$

Figure 3.7 does not appear to show any obvious trend separating surface diving, dipper or plunge diving birds. For an impact velocity of 23.2 m/s, the dipper's im-

pact acceleration is measured to be 383 m/s^2 while those for plunge and surface divers range between $114.3 - 300.1$ m/s^2 and $154.4 - 399.2$ m/s^2, respectively. The highest impact accelerations for all impact velocity tests are recorded for surface divers, specifically the Atlantic Puffin. Other surface divers, however, do not experience relatively high accelerations in comparison. Some plunge divers record higher impact accelerations than surface divers, while others record lower, and vice versa.

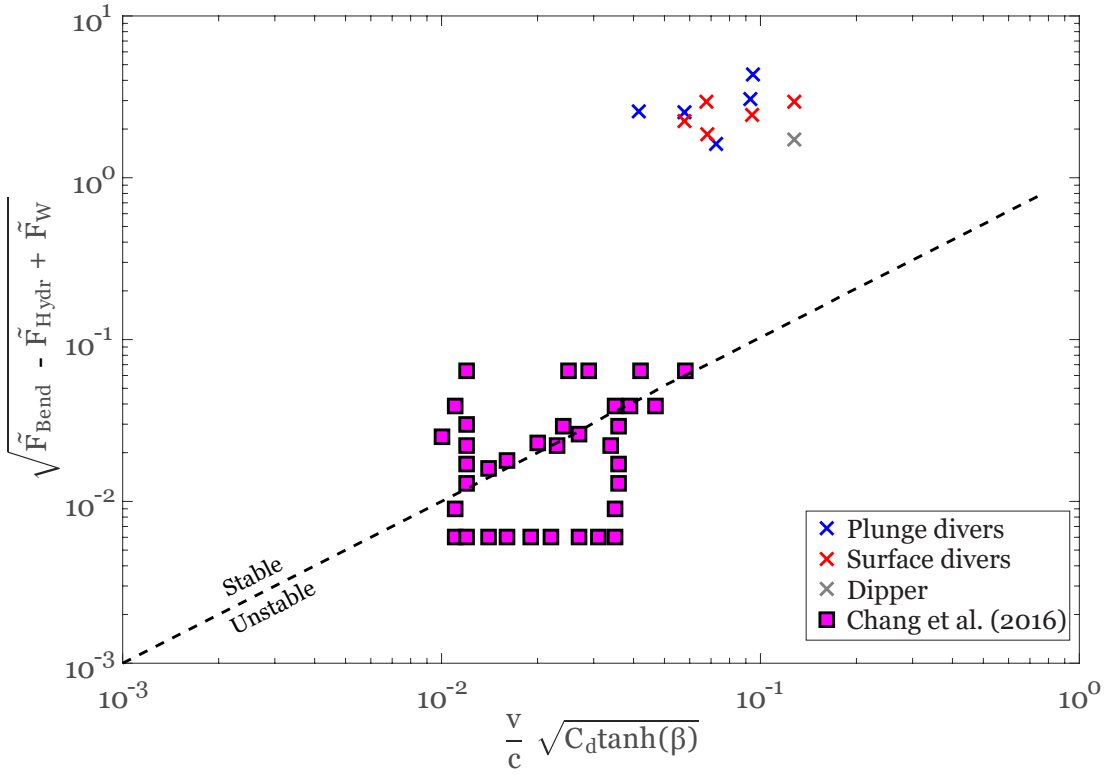

Fig. 3.8: Data from Chang *et al.* [23] experiments identifying stable and unstable regimes using cones and beams as bird head replacements. Data from the current study indicates that all birds tested at the highest impact speed ($v = 23.15$ m/s) dive in the stable regime.

Experiments performed by Chang *et al.* [23] using cones and elastic beams as bird head replicas identified unstable and stable regimes based on whether the beam was

bent or not. Their analysis estimated that Northern Gannets and Brown Boobies dive in a stable regime, capable of diving with impact velocities of up to 24 m/s without incurring any injury. Herein, all of the birds tested are found to dive in the stable regime based on the analysis of Chang *et al.* (calculated at the highest impact velocities, Figure 3.8). This implies that surface divers are capable of diving at high speeds but yet they do not. Equations used are displayed on the axis of the graph where c is the speed of sound in the bird, C_d is the drag coefficient as calculated by Eq. 3.1, β is the highest cone angle of the bird beak, $\tilde{F}_{Bend}$ is calculated after the manner of [23], $-\tilde{F}_{Hydr} + \tilde{F}_W$ is measured indirectly from the accelerometer.

3.4 Impact Duration

Analysis of all individual accelerometer data recorded reveals the impact duration to be different for plunge and surface divers impacting at identical velocities. The impact duration is defined as the time required to reach from zero to maximum acceleration. Figure 3.9 shows the impact duration, Δt, measured in the same manner as by Broglio *et al.* [28], at four different impact velocities for a plunge diver (Northern Gannet) and a surface diver (Common Eider). Shorter impact durations for surface divers can be attributed to obvious differences in their beak shapes. Surface diving birds generally have blunt beak tips with rapidly varying cross-sections whereas plunge divers have sharply pointed beak tips for better water entry characterized by a gradual increase in cross-section (see Appendix A Figure A.1, A.2, A.3). One exception is the Common Loon which, despite being a surface diver, has a sharp tip typical of plunge divers.

3.5 Impact Jerk

An important property considered critical in analyzing the destructive effect of

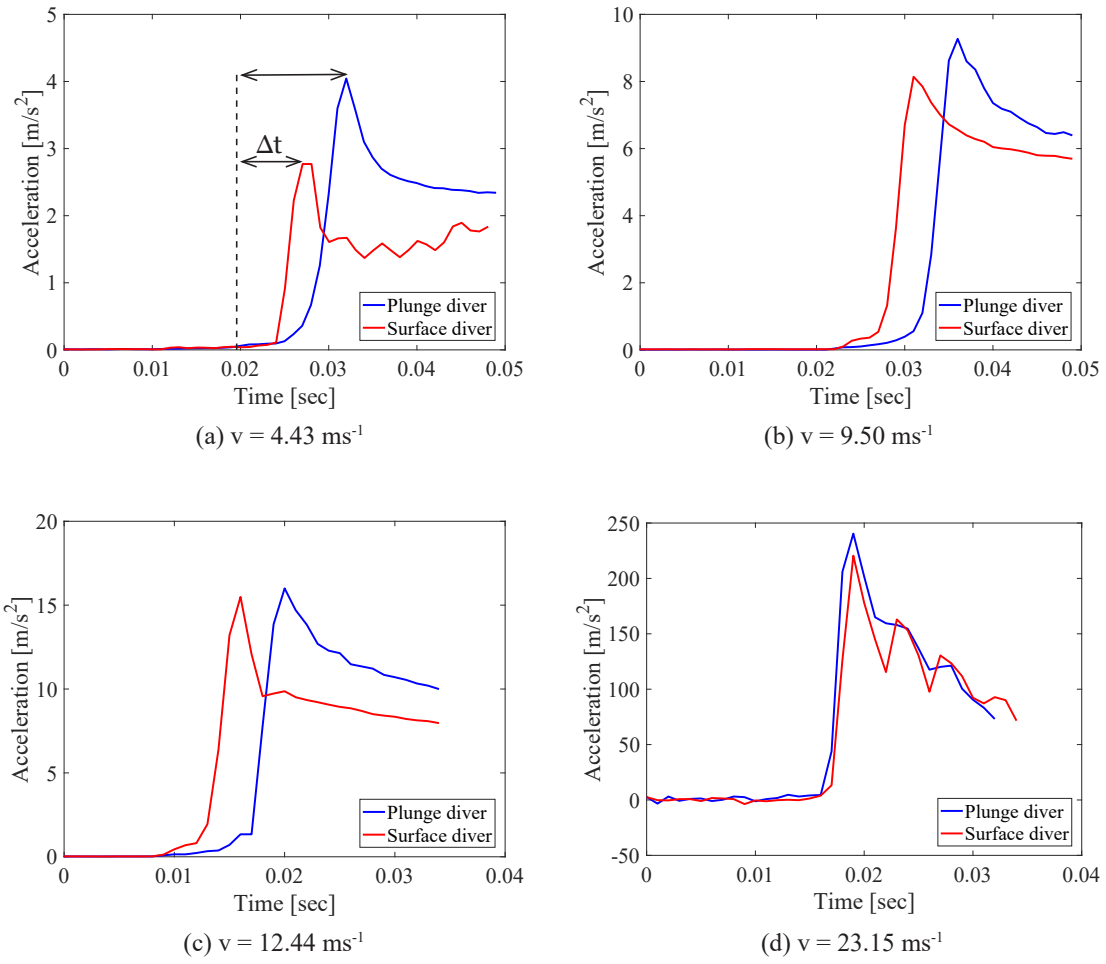

Fig. 3.9: Impact duration, Δt, for a plunge (Northern Gannet) and a surface (Common Eider) diving bird for four different impact velocities marked (a) through (d). As shown in (a), Δt represents a time interval between the start of water entry (marked by the solid line) to the peak of the acceleration curve.

sudden changes in motion is called "jerk". It is defined as the rate of change of acceleration where high jerk values are considered undesirable. Since variations in impact acceleration for bird heads tested herein do not provide a categorical answer as to whether surface divers can dive from high heights or not, the corresponding jerk values are calculated during water entry. The longer impact duration of plunge divers in comparison to surface divers implies a lower jerk during water entry. The

jerk experienced can be non-dimensionalized (J^*) by:

$$J^* = \frac{\Delta a}{\Delta t} . \frac{m}{\frac{1}{2}\rho g v A} \tag{3.3}$$

where Δa is the change in acceleration during impact, Δt is the impact duration, m is the total mass of the projectile and IMU, ρ is the density of water, v is the impact velocity and A is the area of the neck. The non-dimensional jerk values for all bird heads tested in this study are shown in Figure 3.10.

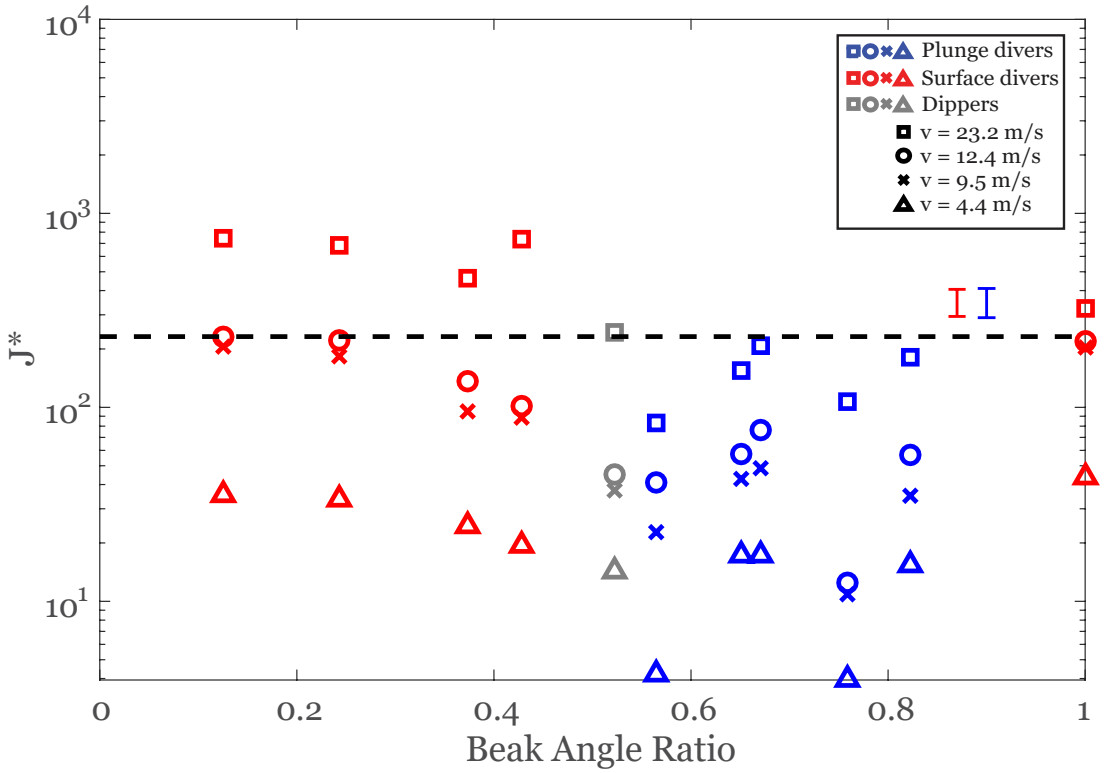

Fig. 3.10: Non-dimensional jerk J^* vs beak angle ratios of the bird models used for four different impact velocities. The error bars show maximum calculation errors and the dotted line represents the theoretical safe limit based on human injury data.

Surface and plunge divers have similar J^* values for low impact speeds but distinctions arise as velocity increases. The dipper (Herring Gull) is found to have a J^* value similar to those of plunge divers. This is expected, as Herring Gulls are often observed to make plunge dives [16, 17]. The dotted line represents a theoretical safe limit calculated from Eq. 3.3 based on data obtained from human injury experiments, due to the lack of literature on the safe limits of bird water entry impact. According to Hill [29], the inherent strength of a contracting voluntary muscle fiber is roughly constant and is independent of the size of the animal. The maximum stress that a mammalian muscle can exert is found to be 0.35 MPa [30] and that of a bird muscle is found to be 0.30 MPa [31], which are close enough to support Hill's [29] conclusion. Thus, considering that birds and humans have similar muscle strength, we can non-dimensionalize information from human water impact injury studies to calculate the safe limit for J^* of birds. Studies investigating different cases of humans jumping into water at high impact speeds determined the critical impact velocity for survival. Kumar & Norfleet [32] reported a critical impact velocity of 35 m/s for human survival in free fall impacts onto water, whereas Snyder [33] obtained a value of 30.5 m/s. Of the two critical impact velocities reported, we use $v = 30.5$ m/s. Similarly, experiments on athletes have been conducted to determine the critical impact acceleration and impact duration that could result in a concussion. Pellman *et al.* [34] proposed that a linear acceleration of $686 - 735.8$ m/s^2 for an impact duration of 15 ms is necessary to induce a concussion in humans. Withnall *et al.* [35] however concluded that there is a 50% chance of injury at an acceleration of 765.2 m/s^2 which is used here to obtain the theoretical safe limit. According to this limiting non-dimensional jerk, any value that falls below the dotted line is considered safe and anything above is unsafe. While surface divers appear divided by the line, all plunge divers fall within the safe region even for the highest impact velocities tested. The dipper is also in

the safe region of J^* values, having a beak angle ratio close to those obtained for plunge diving birds (Figure 3.5(a)). Surface divers diving at lower impact velocities are found to be in or near the safe region, still being close to the limit. However, none of the surface divers fall in the safe region when impacting at 23.2 m/s. The proposed safety limit can explain why surface divers do not dive from high heights and risk breaking their necks, which indicates that J^* could be a deciding factor in determining whether a bird can dive or not.

CHAPTER 4

CONCLUSIONS

This study presents the initial water-entry dynamics of diving birds to understand why plunge divers can dive into water at high speeds but surface divers do not. An embedded Inertial Measurement Unit (IMU) is used to measure the impact accelerations of eleven 3D printed bird head models (five plunge diving, one dipper, and five surface diving birds) for impact velocities ranging between $4.4-23.2\ m/s$. Surface divers are noted to have smaller beak angle ratios ($0.125-0.428$) than plunge divers ($0.565-0.822$), with the exception of the Merganser (1.0) having a nearly symmetric beak tip. Impact accelerations experienced for the highest impact velocity by plunge divers ($114.3-300.1\ m/s^2$), dipper ($383\ m/s^2$) and surface divers ($154.4-399.2\ m/s^2$) are not distinguishable. Since impact accelerations cannot discern between surface and plunge diving birds, a non-dimensional jerk (J^*) having a safe limit based on past human injury and survival results is introduced. At the highest impact speeds tested, surface divers are found to be associated with J^* values exceeding the safe limit while all plunge divers and the dipper are not. Thus, the non-dimensional jerk provides a potential measurement to explain why surface diving birds avoid plunge diving acrobatic techniques.

Although the conclusions of this study provide a good understanding of why surface divers do not dive from higher heights but plunge divers do, further work can be done to improve and validate the results. A principal area of focus for future work is to refine the use of the IMU, especially to reduce the error associated with the hardware and to increase the sampling frequency. Instead of using only the bird head, the whole body of the bird can be printed and used as the projectile. This will

be expensive but it will provide more accurate results. An even better option will be to use the real body of a dead bird, or put an IMU with high sampling frequnecy on a live bird and track its motion. Numerical studies focused on the free-surface impact of diving birds can also be performed to compare with the findings of the IMU.

REFERENCES

[1] May, A., "Water entry and the cavity-running behavior of missiles," Tech. rep., DTIC Document, 1975.

[2] Truscott, T. T., Epps, B. P., and Belden, J., "Water entry of projectiles," *Annual review of fluid mechanics*, Vol. 46, 2014, pp. 355–378.

[3] Shiffman, N. and Spencer, D., "The force of impact on a sphere striking a water surface," 1945.

[4] Moghisi, M. and Squire, P., "An experimental investigation of the initial force of impact on a sphere striking a liquid surface," *Journal of Fluid Mechanics*, Vol. 108, 1981, pp. 133–146.

[5] May, A. and Woodhull, J. C., "The virtual mass of a sphere entering water vertically," *Journal of Applied Physics*, Vol. 21, No. 12, 1950, pp. 1285–1289.

[6] Truscott, T. T., Epps, B. P., and Techet, A. H., "Unsteady forces on spheres during free-surface water entry," *Journal of Fluid Mechanics*, Vol. 704, 2012, pp. 173–210.

[7] Shepard, T., Abraham, J., Schwalbach, D., Kane, S., Siglin, D., and Harrington, T., "Velocity and density effect on impact force during water entry of sphere," *J. Geophys. Remote Sens*, Vol. 3, No. 129, 2014, pp. 2169–0049.

[8] Eroshin, V. A., Romanenkov, N. I., Serebryakov, I. V., and Yakimov, Y. L., "Hydrodynamic forces produced when blunt bodies strike the surface of a compressible fluid," *Fluid Dynamics*, Vol. 15, No. 6, 1980, pp. 829–835.

[9] Bodily, K. G., Carlson, S. J., and Truscott, T. T., "The water entry of slender axisymmetric bodies," *Physics of Fluids*, Vol. 26, No. 7, 2014, pp. 072108.

[10] Korobkin, A. and Pukhnachov, V., "Initial stage of water impact," *Annual Review of Fluid Mechanics*, Vol. 20, No. 1, 1988, pp. 159–185.

[11] Tveitnes, T., Fairlie-Clarke, A., and Varyani, K., "An experimental investigation into the constant velocity water entry of wedge-shaped sections," *Ocean Engineering*, Vol. 35, No. 14, 2008, pp. 1463–1478.

[12] Ropert-Coudert, Y., Grmillet, D., Ryan, P., Kato, A., Naito, Y., and Le Maho, Y., "Between air and water: the plunge dive of the Cape Gannet Morus capensis," *Ibis*, Vol. 146, No. 2, 2004, pp. 281–290.

[13] Lee, D. N. and Reddish, P. E., "Plummeting gannets: a paradigm of ecological optics," *Nature*, Vol. 293, No. 5830, Sept. 1981, pp. 293–294.

[14] Brierley, A. S. and Fernandes, P. G., "Diving Depths of Northern Gannets: Acoustic Observations of Sula Bassana from an Autonomous Underwater Vehicle," *The Auk*, Vol. 118, No. 2, April 2001, pp. 529–534.

[15] Castro, P. and Huber, M., *Marine Biology: Ninth Edition*, McGraw-Hill Higher Education, 2012.

[16] Nicolaas A. M. Verbeek, "Comparative Feeding Behavior of Immature and Adult Herring Gulls," *The Wilson Bulletin*, Vol. 89, No. 3, 1977, pp. 415–421.

[17] Sibly, R. M. and McCleery, R. H., "The Distribution between Feeding Sites of Herring Gulls Breeding at Walney Island, U.K." *Journal of Animal Ecology*, Vol. 52, No. 1, 1983, pp. 51–68.

[18] Adams, N. J. and Walter, C. B., "Maximum Diving Depths of Cape Gannets," *The Condor*, Vol. 95, No. 3, 1993, pp. 734–736.

[19] Le Corre, M., "Diving Depths of Two Tropical Pelecaniformes: The Red-Tailed Tropicbird and the Red-Footed Booby," *The Condor*, Vol. 99, No. 4, 1997, pp. 1004–1007.

[20] Garthe, S., Benvenuti, S., and Montevecchi, W. A., "Pursuit plunging by northern gannets (Sula bassana) "feeding on capelin (Mallotus villosus)"," *Proceedings of the Royal Society of London B: Biological Sciences*, Vol. 267, No. 1454, 2000, pp. 1717–1722.

[21] Machovsky-Capuska, G. E., Dwyer, S. L., Alley, M. R., Stockin, K. A., and Raubenheimer, D., "Evidence for fatal collisions and kleptoparasitism while plungediving in Gannets," *Ibis*, Vol. 153, No. 3, 2011, pp. 631–635.

[22] Wang, T., Yang, X., Liang, J., Yao, G., and Zhao, W., "CFD based investigation on the impact acceleration when a gannet impacts with water during plunge diving," *Bioinspiration & biomimetics*, Vol. 8, No. 3, 2013, pp. 036006.

[23] Chang, B., Croson, M., Straker, L., Gart, S., Dove, C., Gerwin, J., and Jung, S., "How seabirds plunge-dive without injuries," *Proceedings of the National Academy of Sciences*, Vol. 113, No. 43, Oct. 2016, pp. 12006–12011.

[24] Alderfer, J., *National geographic complete birds of North America*, National Geographic Books, 2014.

[25] Perrins, C., *The New Encyclopedia of Birds*, Oxford University Press, 2003.

[26] Baldwin, J. L., "Vertical water entry of cones," Tech. rep., DTIC Document, 1971.

[27] Grumstrup, T., Keller, J. B., and Belmonte, A., "Cavity ripples observed during the impact of solid objects into liquids," *Physical review letters*, Vol. 99, No. 11, 2007, pp. 114502.

[28] Broglio, S. P., Sosnoff, J. J., Shin, S., He, X., Alcaraz, C., and Zimmerman, J., "Head impacts during high school football: a biomechanical assessment," *Journal of athletic training*, Vol. 44, No. 4, 2009, pp. 342–349.

[29] Hill, A. V., "The dimensions of animals and their muscular dynamics," *Science Progress (1933-)*, Vol. 38, No. 150, 1950, pp. 209–230.

[30] Madden, J. D., Vandesteeg, N. A., Anquetil, P. A., Madden, P. G., Takshi, A., Pytel, R. Z., Lafontaine, S. R., Wieringa, P. A., and Hunter, I. W., "Artificial muscle technology: physical principles and naval prospects," *IEEE Journal of oceanic engineering*, Vol. 29, No. 3, 2004, pp. 706–728.

[31] Pennycuick, C., "Stress and strain in the flight muscles as constraints on the evolution of flying animals," *Journal of biomechanics*, Vol. 29, No. 5, 1996, pp. 577–581.

[32] Kumar, K. V. and Norfleet, W. T., "Issues on human acceleration tolerance after long-duration space flights," 1992.

[33] Snyder, R. G., "Survival of High-velocity Free-falls in Water," Tech. rep., DTIC Document, 1965.

[34] Pellman, E. J., Viano, D. C., Tucker, A. M., Casson, I. R., and Waeckerle, J. F., "Concussion in professional football: reconstruction of game impacts and injuries," *Neurosurgery*, Vol. 53, No. 4, 2003, pp. 799–814.

[35] Withnall, C., Shewchenko, N., Gittens, R., and Dvorak, J., "Biomechanical investigation of head impacts in football," *British journal of sports medicine*, Vol. 39, No. suppl 1, 2005, pp. i49–i57.

APPENDICES

APPENDIX A

Bird Beak Angles

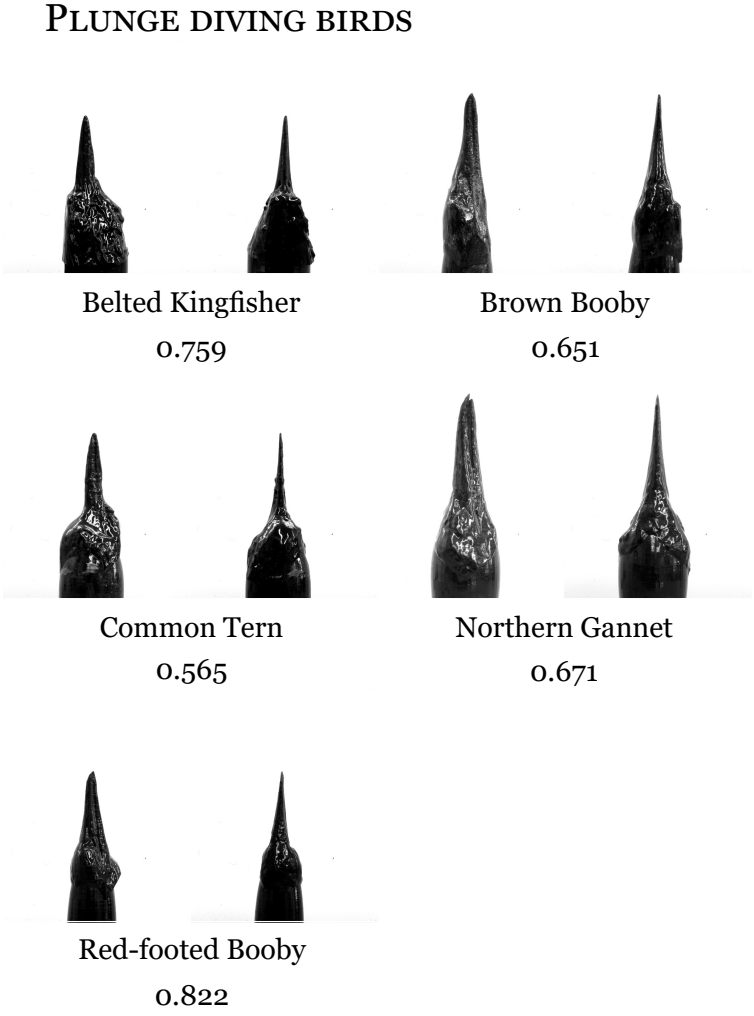

Fig. A.1: Side and top view images of all the plunge diving birds used. Beak angle ratios are labeled below each bird name and calculated from side and top beak angles. The Belted Kingfisher and the Common Tern have been magnified 1.5 times during 3D printing to accommodate the IMU inside the printed model, which does not affect the beak angle ratio.

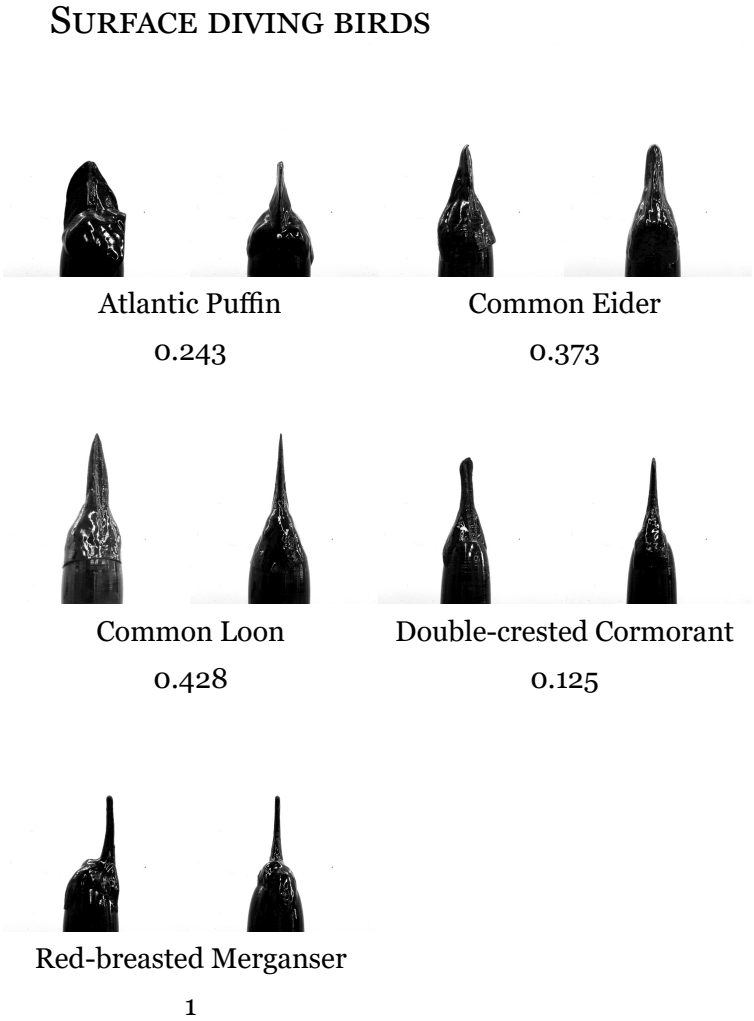

Fig. A.2: Side and top view images of all the surface diving birds used. Beak angle ratios are labeled below each bird name and calculated from side and top beak angles. The Atlantic Puffin have been magnified 1.5 times during 3D printing to accommodate the IMU inside the printed model, which does not affect the beak angle ratio.

Dipper

Herring Gull

0.522

Fig. A.3: Side and top view images of the dipper. Beak angle ratio is labeled below the bird name and calculated from side and top beak angles.

APPENDIX B

Oscillation Frequency

Table B.1: Oscillation frequencies in Hz after pinch-off of all the bird heads at each impact velocity.

Name of Bird	v = 4.4 m/s	9.5 m/s	12.4 m/s	23.2 m/s
Plunge Diving Birds				
Belted Kingfisher	107.70	81.76	73.73	59.36
Brown Booby	116.70	95.50	80.36	59.83
Common Tern	125.32	90.91	75.89	87.63
Northern Gannet	125.00	85.37	74.77	48.03
Red-footed Booby	115.10	94.34	84.11	68.75
Dipper				
Herring Gull	101.2	88.05	71.15	53.57
Surface Diving Birds				
Atlantic Puffin	123.10	93.96	82.95	55.28
Common Eider	125.80	95.54	79.44	76.92
Double-crested Cormorant	109.20	94.70	84.10	67.04
Common Loon	126.40	84.40	73.06	51.95
Red-breasted Merganser	114.30	97.40	86.67	97.20

APPENDIX C

Impact Acceleration and Duration Plots

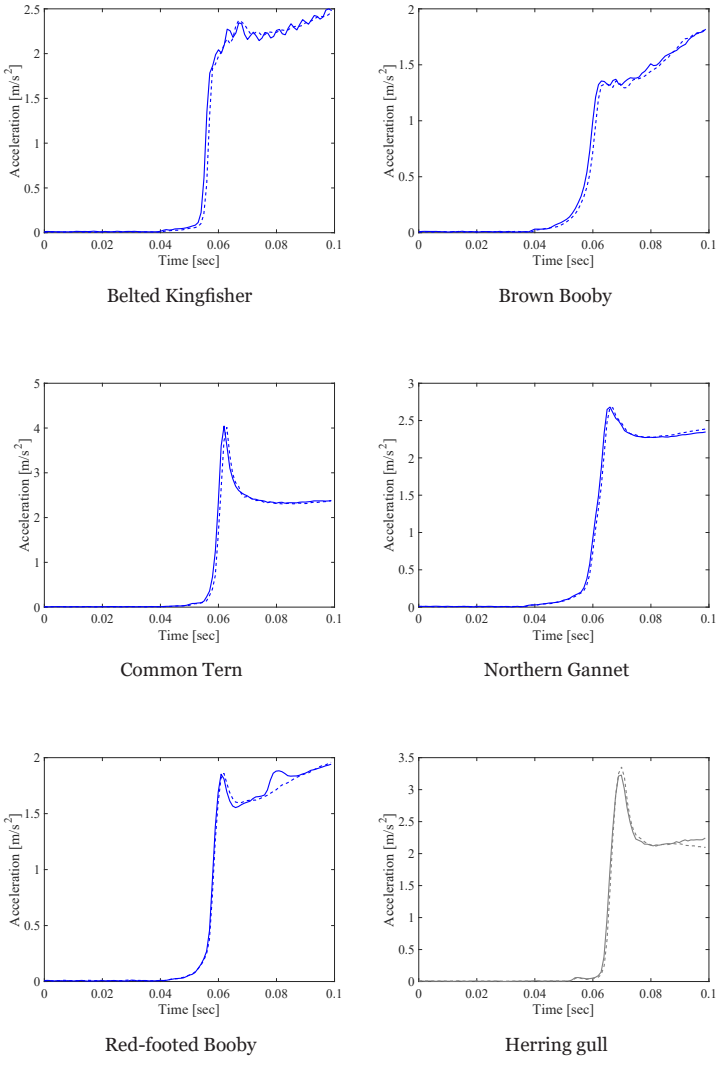

Fig. C.1: Impact acceleration and duration, Δt, for multiple drops of all the plunge diving birds and the dipper (last plot) used for an impact velocity of $v = 4.4\ m/s$.

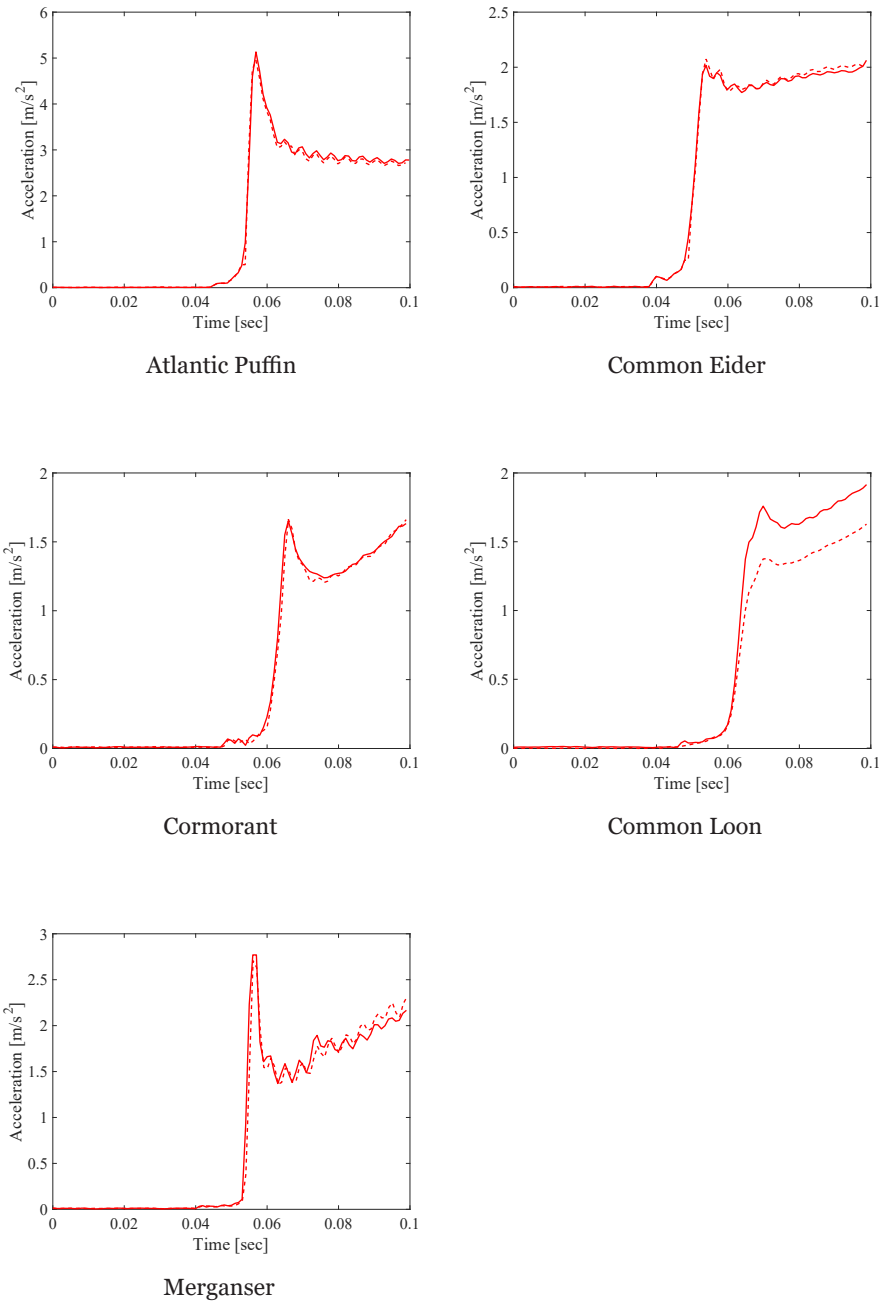

Fig. C.2: Impact acceleration and duration, Δt, for multiple drops of all the surface diving birds used for an impact velocity of $v = 4.4\ m/s$.

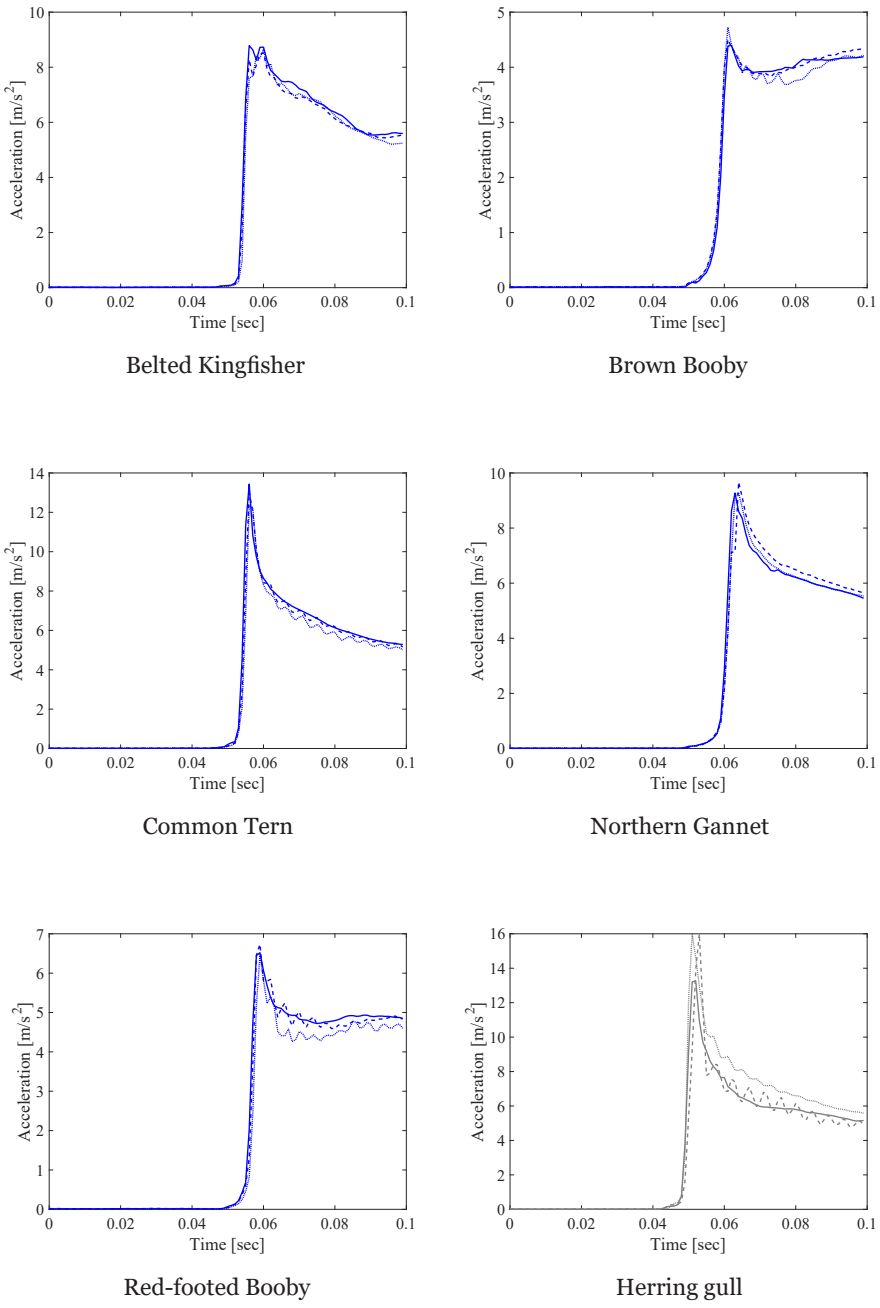

Fig. C.3: Impact acceleration and duration, Δt, for multiple drops of all the plunge diving birds and the dipper (last plot) used for an impact velocity of $v = 9.5\ m/s$.

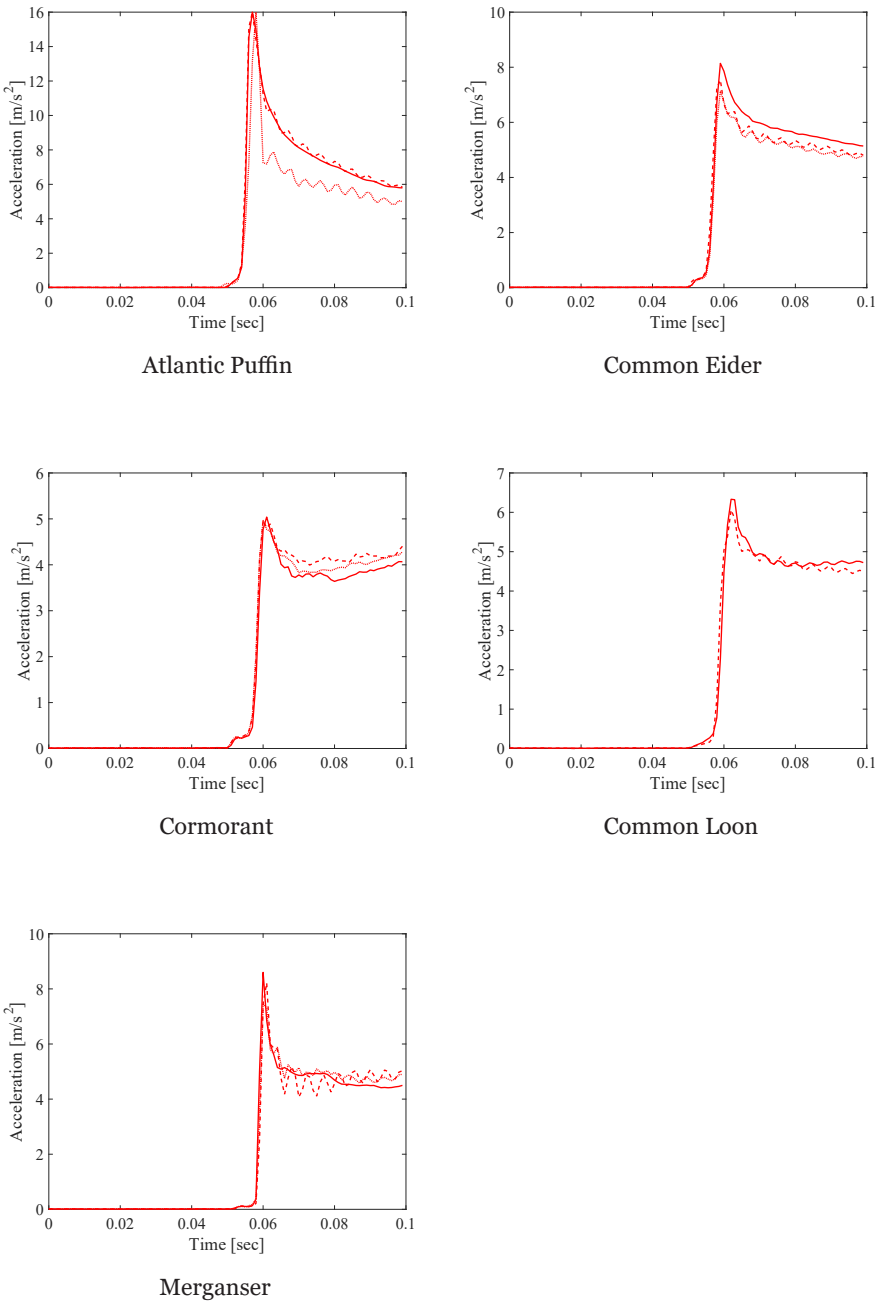

Fig. C.4: Impact acceleration and duration, Δt, for multiple drops of all the surface diving birds used for an impact velocity of $v = 9.5\ m/s$.

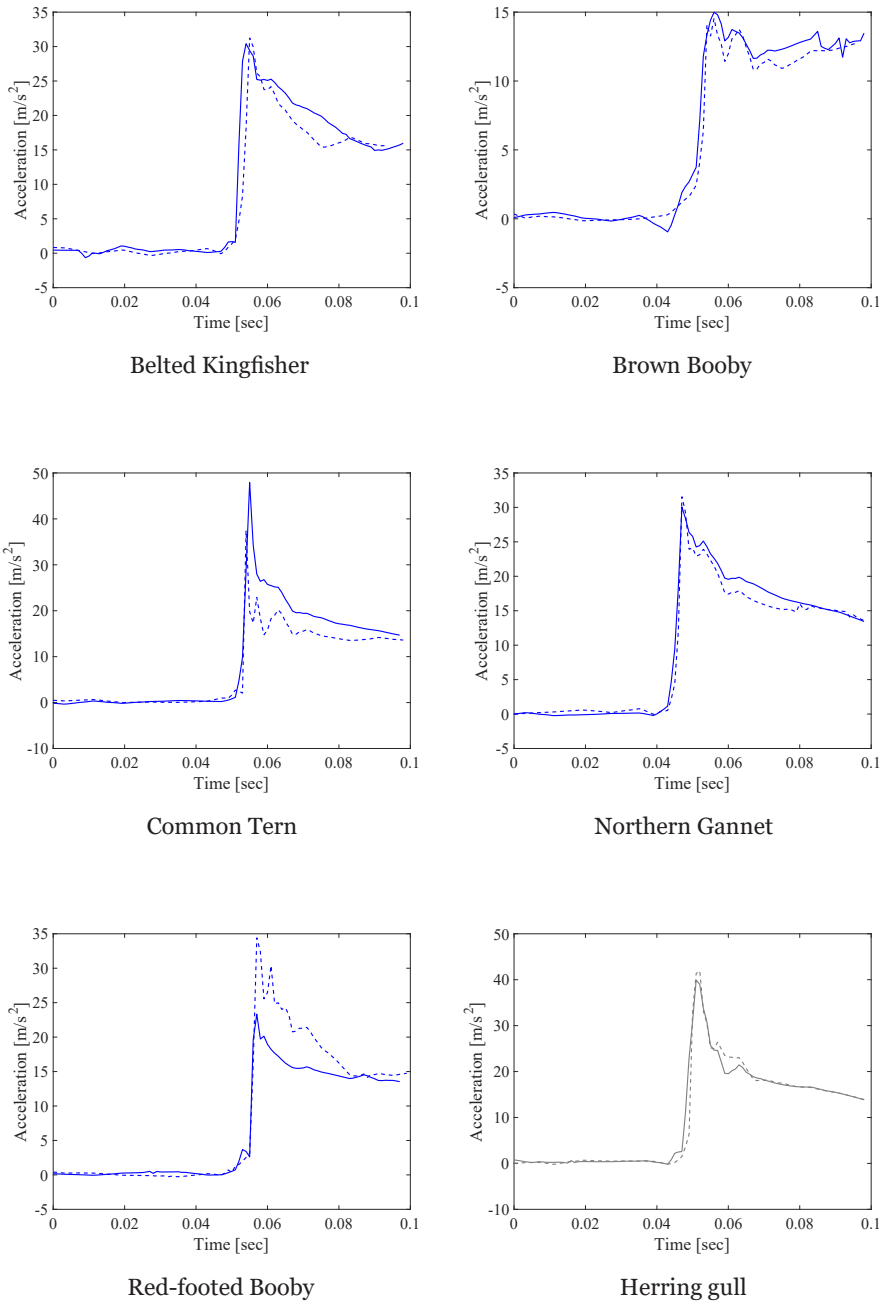

Fig. C.5: Impact acceleration and duration, Δt, for multiple drops of all the plunge diving birds and the dipper (last plot) used for an impact velocity of $v = 12.4\ m/s$.

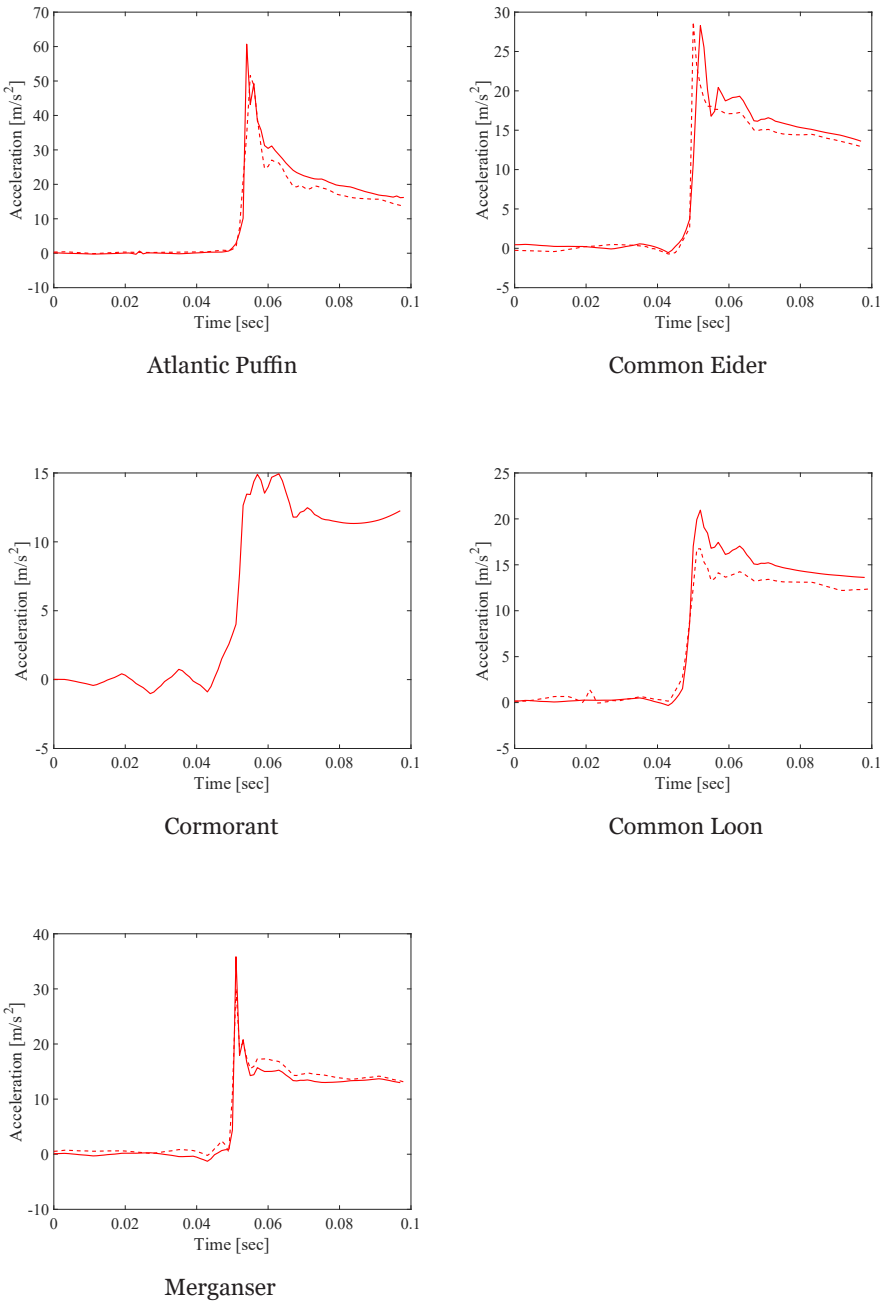

Fig. C.6: Impact acceleration and duration, Δt, for multiple drops of all the surface diving birds used for an impact velocity of $v = 12.4\ m/s$.

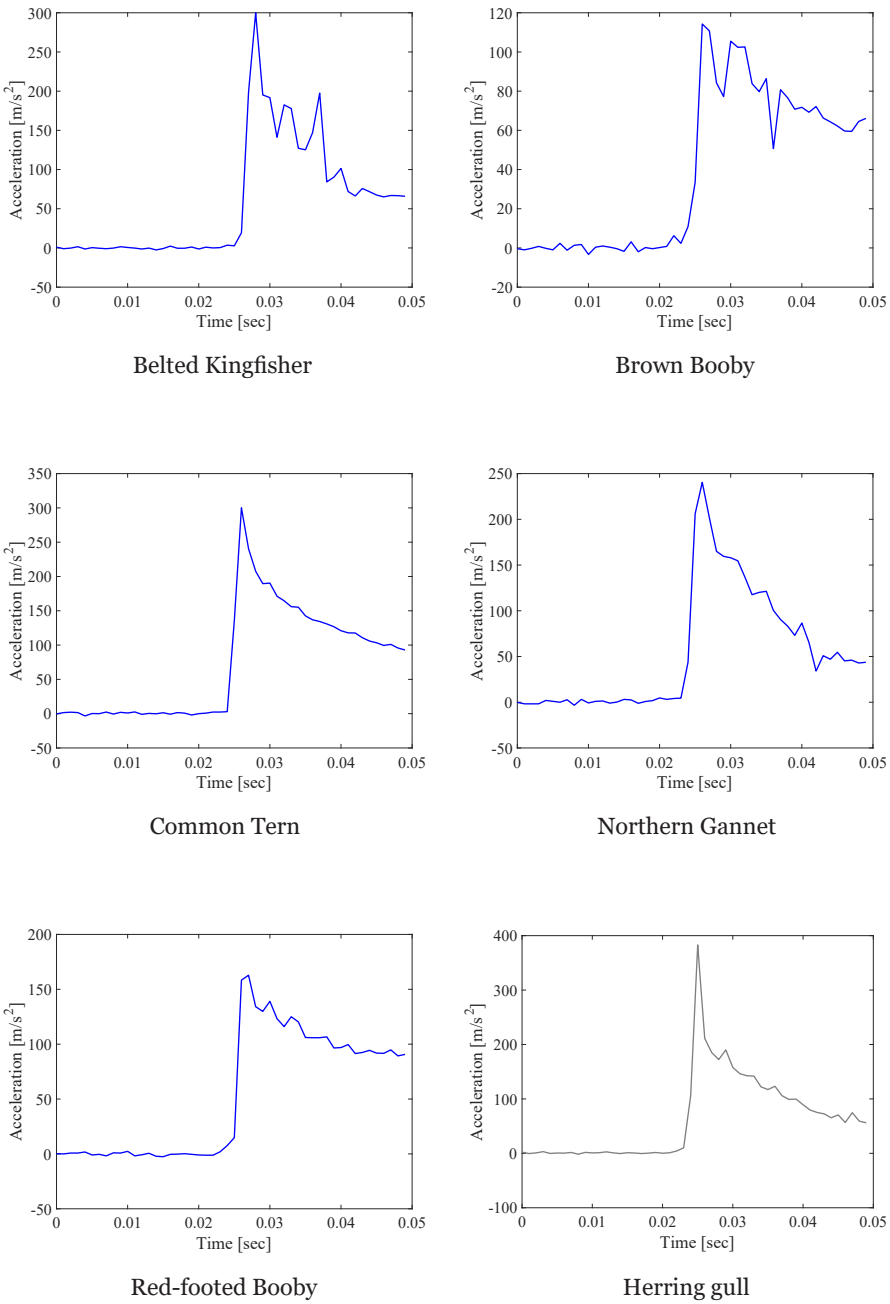

Fig. C.7: Impact acceleration and duration, Δt, of all the plunge diving birds and the dipper (last plot) used for an impact velocity of $v = 23.2\ m/s$.

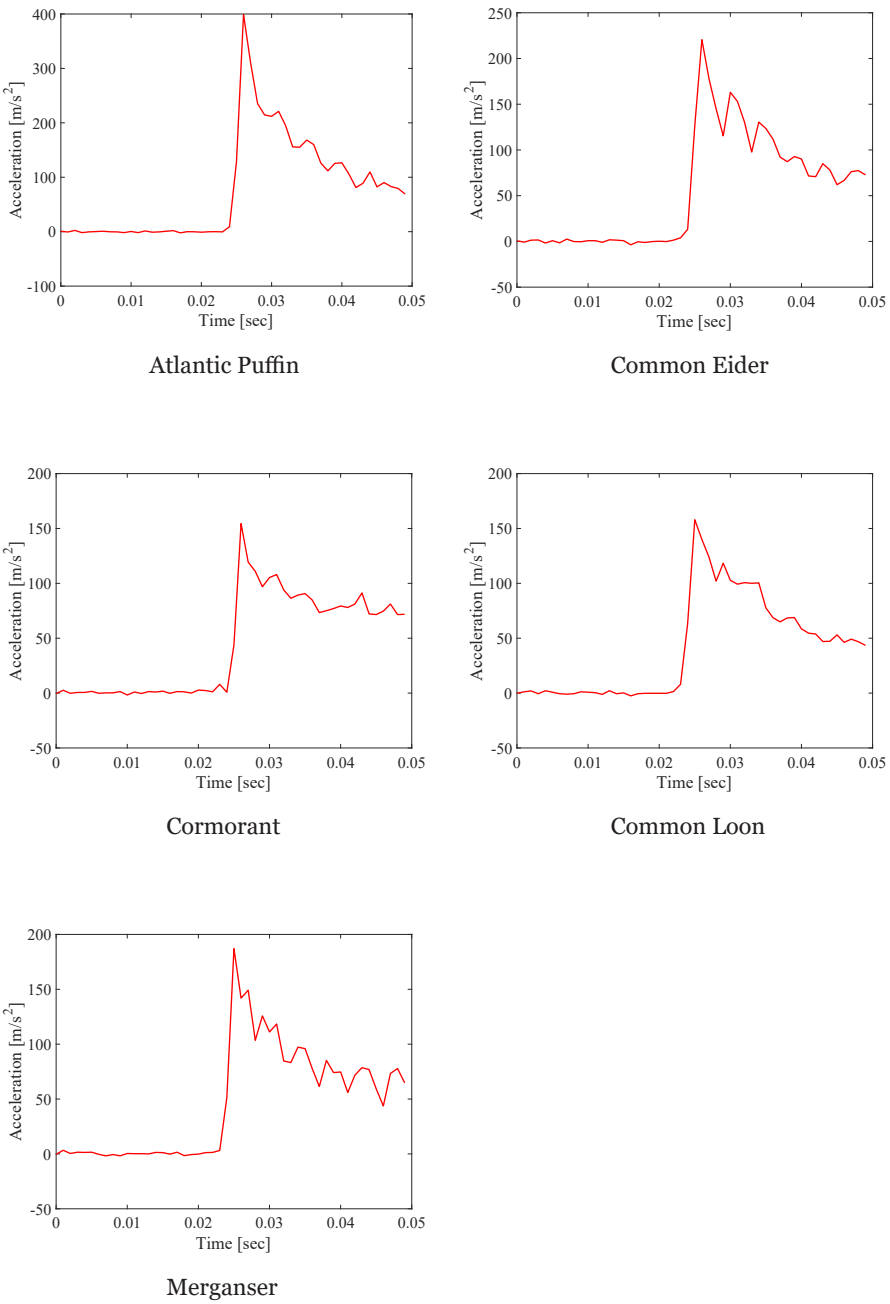

Fig. C.8: Impact acceleration and duration, Δt, of all the surface diving birds used for an impact velocity of $v = 23.2\ m/s$.